Colloquium: Quantum heat transport in condensed matter systems

Jukka P. Pekola*

Pico Group, QTF Centre of Excellence, School of Science, Department of Applied Physics, Aalto University, P.O. Box 13500, 00076 Aalto, Finland and Moscow Institute of Physics and Technology, 141700 Dolgoprudny, Russia

Bayan Karimi†

Pico Group, QTF Centre of Excellence, School of Science, Department of Applied Physics, Aalto University, P.O. Box 13500, 00076 Aalto, Finland

(published 5 October 2021)

In this Colloquium recent advances in the field of quantum heat transport are reviewed. This topic has been investigated theoretically for several decades, but only during the past 20 years have experiments on various mesoscopic systems become feasible. A summary of the theoretical basis for describing heat transport in one-dimensional channels is first provided. The main experimental investigations of quantized heat conductance due to phonons, photons, electrons, and anyons in such channels are then presented. These experiments are important for understanding the fundamental processes that underlie the concept of a heat conductance quantum for a single channel. An illustration of how one can control the quantum heat transport by means of electric and magnetic fields, and how such tunable heat currents can be useful in devices, is first given. This lays the basis for realizing various thermal device components such as quantum heat valves, rectifiers, heat engines, refrigerators, and calorimeters. Also of interest are fluctuations of quantum heat currents, both for fundamental reasons and for optimizing the most sensitive thermal detectors; at the end of the Colloquium the status of research on this topic is given.

DOI: 10.1103/RevModPhys.93.041001

CONTENTS

*jukka.pekola@aalto.fi
†bayan.karimi@aalto.fi

I. INTRODUCTION

In this Colloquium we present advances on fundamental aspects of thermal transport in the regime where quantum effects play an important role. Usually this means dealing with atomic scale structures or low temperatures, or a combination of the two. The seminal theoretical work by Pendry (1983) presented, almost 40 years ago, the important observation that a ballistic channel for any type of a carrier can transport heat at the rate given by the so-called quantum of thermal conductance G_Q. During this millenium the theoretical ideas have developed into a plethora of experiments in systems involving phonons, electrons, photons, and recently particles obeying fractional statistics. We give an overview of these experiments backed by the necessary theoretical framework. The question as to whether or not a channel is ballistic, and under what conditions, is interesting as such, but it also has more practical implications. If one can control the degree of ballisticity,

i.e., the transmission coefficient of the channel, one can turn the heat current on and off. Such quantum heat switches, or heat valves as they are often called, are discussed in this Colloquium as well. Furthermore, the heat current via a quantum element in an asymmetric structure can violate reciprocity in the sense that rectification of the heat current becomes possible. The bulk of the Colloquium deals with the time average (mean) of the heat current. Yet the fluctuations of this quantity are interesting, and they provide a yardstick for the minimal detectable power and for the ultimate energy resolution of a thermal detector. We discuss such a noise and its implications in ultrasensitive detection.

The Colloquium begins with a theoretical discussion of thermoelectric transport in one-dimensional channels in Sec. II. In Sec. III we present the concept and method of how to measure heat currents in general. Section IV reviews the central elements of the experimental setups. After these general sections, we move on to heat transport in different physical systems: phonons in Sec. V, electrons and fractional charges in Sec. VI, and photons in Sec. VII, including some detailed theoretical discussion within the sections. Section VIII presents experimental results on heat control by external fields. In Sec. IX we move on to the discussion of a superconducting qubit as a tunable element in quantum thermodynamics. Section X gives an account of both theoretical expectations and the experimental status of the heat current noise and associated fluctuations of the effective temperature. Section XI concludes the Colloquium with a summary and outlook including the prospects for useful thermal devices and some interesting physical questions related to quantum heat transport.

II. THERMOELECTRIC TRANSPORT IN A ONE-DIMENSIONAL (1D) CHANNEL

Consider two infinite reservoirs with temperature T_i and chemical potential μ_i that are connected adiabatically via a conductor as shown schematically in Fig. 1. Here the subscripts $i = \mathrm{L}, \mathrm{R}$ represent the left and right, respectively. Based on Landauer theory (Landauer, 1981; Sivan and Imry, 1986; Butcher, 1990), the charge and energy currents I and $\mathcal{J}$ between the two reservoirs (from L to R) are given for a 1D conductor by

$$I = q\sum_n \int_0^\infty \frac{dk}{2\pi} v_n(k)(\vartheta_\mathrm{L} - \vartheta_\mathrm{R})\mathcal{T}_n(k),$$
$$\mathcal{J} = \sum_n \int_0^\infty \frac{dk}{2\pi} \varepsilon_n(k) v_n(k)(\vartheta_\mathrm{L} - \vartheta_\mathrm{R})\mathcal{T}_n(k), \qquad (1)$$

where q is the particle charge, $\sum_n$ presents the sum over independent modes in the conductor, and $\varepsilon_n(k)$ and $v_n(k)$ indicate the energy and the velocity of the particles with wave vector k, respectively. $\mathcal{T}_n(k)$ indicates the particle transmission probability through the conductor via the channel; for ballistic transport $\mathcal{T}_n(k) \equiv 1$, and $\vartheta_{\mathrm{L,R}}$ represents the statistical distribution functions in each reservoir. Changing the variable from wave vector to energy via the definition of the velocity $v_n(k) = (1/\hbar)\partial\varepsilon_n(k)/\partial k$, we have

$$I = \frac{q}{h}\sum_n \int_{\varepsilon(0)}^\infty d\varepsilon[\vartheta_\mathrm{L}(\varepsilon) - \vartheta_\mathrm{R}(\varepsilon)]\mathcal{T}_n(\varepsilon),$$
$$\mathcal{J} = \frac{1}{h}\sum_n \int_{\varepsilon(0)}^\infty d\varepsilon\,\varepsilon[\vartheta_\mathrm{L}(\varepsilon) - \vartheta_\mathrm{R}(\varepsilon)]\mathcal{T}_n(\varepsilon), \qquad (2)$$

where $\varepsilon(0) \equiv \varepsilon$ for $k = 0$. Equations (2) constitute the basis of thermoelectrics, with a linear response for electrical and thermal conductance and for Seebeck and Peltier coefficients.

Now we analytically solve these equations for a ballistic contact $\mathcal{T}_n(\varepsilon) \equiv 1$ with the most common carriers, that is, fermions and bosons. For fermions $\vartheta_i(\varepsilon) \equiv f_i(\varepsilon - \mu_i) = 1/(1 + e^{\beta_i(\varepsilon-\mu_i)})$ is the Fermi distribution function for each reservoir, with the inverse temperature $\beta_i = 1/(k_B T_i)$. Note that we have taken the Fermi energy as the zero of ε, meaning that $\varepsilon(0) \to -\infty$. In this case at temperature T, with only the chemical potential difference eV across the contact, the charge current is

$$I = N\frac{e}{h}\int_{-\infty}^\infty d\varepsilon[f(\varepsilon) - f(\varepsilon - eV)] = N\frac{e^2V}{h}. \qquad (3)$$

Here N replacing the sum represents the number of current carrying modes in the conductor with $q \equiv e$. The electrical conductance $G = dI/dV$ is then

$$G = Ne^2/h, \qquad (4)$$

which is the quantization of electrical conductance. The thermal conductance for fermions can be obtained from the heat flux $\dot{Q} = \mathcal{J}$ when both reservoirs have the same chemical potential. The heat current across the ballistic contact is then

$$\dot{Q} = \frac{1}{h}\sum_n \int_{-\infty}^\infty d\varepsilon\,\varepsilon[f_\mathrm{L}(\varepsilon) - f_\mathrm{R}(\varepsilon)]. \qquad (5)$$

The subtle differences between energy and heat currents are discussed in Sec. IV.B. In this Colloquium we focus mainly on

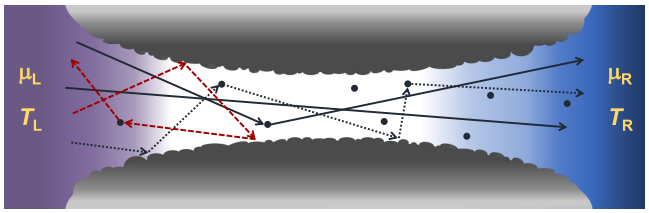

FIG. 1. Artistic representation of a generic conductor between two reservoirs. Both particles and heat are transported through. Depending on the strength and type of scattering at the impurities (dots) and walls, one can have either ballistic or diffusive transport. Here μ_i and T_i, for $i = \mathrm{L}, \mathrm{R}$, are the chemical potential and temperature of each reservoir on the left and right, respectively.

thermal conductance at equilibrium ($T_L = T_R \equiv T$), i.e., on $G_{th}(T) \equiv d\dot{Q}/dT_L|_T$. The thermal conductance is then

$$G_{th}^{(f)} = N\frac{1}{h}\frac{1}{k_B T^2}\int_{-\infty}^{\infty} d\varepsilon\, \varepsilon^2 f(\varepsilon)[1-f(\varepsilon)] = N\frac{\pi^2 k_B^2}{3h}T \equiv N G_Q, \tag{6}$$

where the superscript (f) stands for fermions and

$$G_Q \equiv \frac{\pi^2 k_B^2}{3h}T \tag{7}$$

is the thermal conductance quantum. The ratio of the thermal and electrical conductances satisfies the Wiedemann-Franz law $G_{th}^{(f)}/G = \mathcal{L}T$, where the Lorenz number is $\mathcal{L} = \pi^2 k_B^2/(3e^2)$ (Ashcroft and Mermin, 1976).

We obtain the following thermal conductance for bosons $G_{th}^{(b)}$ with the same procedure but with the distribution function $\vartheta_{R,L}(\varepsilon) \equiv n_{R,L}(\varepsilon) = 1/(e^{\beta_{R,L}\varepsilon} - 1)$ in Eq. (2):

$$G_{th}^{(b)} = \frac{\hbar^2}{2\pi k_B T^2}\sum_n \int_0^{\infty} d\omega \frac{\omega^2 e^{\beta\hbar\omega}}{(e^{\beta\hbar\omega}-1)^2}\mathcal{T}_n(\omega). \tag{8}$$

Here $\varepsilon = \hbar\omega$ is the energy of each boson. For a single fully transmitting channel $\mathcal{T}_n(\omega) = 1$, we then again obtain

$$G_{th}^{(b)} = G_Q. \tag{9}$$

Fermions and bosons naturally form the playground for most experimental realizations in the quantum regime. Yet the previous result for a ballistic channel $G_{th} = G_Q$ is far more general. As demonstrated by Rego and Kirczenow (1999) and Blencowe and Vitelli (2000), this expression is invariant even if one introduces carriers with arbitrary fractional exclusion statistics (Wu, 1994). Recently Banerjee *et al.* (2017) experimented on a fractional quantum Hall system addressing this universality of the thermal conductance quantum for anyons.

III. THERMAL CONDUCTANCE: MEASUREMENT ASPECTS

A. Principles of measuring heat currents

For determining thermal conductance one needs in general a measurement of local temperature. Suppose that an absorber like the one in Fig. 2(a) is heated at a constant power $\dot{Q}$. By continuity, the relation between $\dot{Q}$ and temperature T of the absorber with respect to the bath temperature T_0 can be written as

$$\dot{Q} = \mathcal{K}(T^n - T_0^n), \tag{10}$$

where $\mathcal{K}$ and n are constants characteristic of the absorber and the process of thermalization. For the most common process in metals, the coupling of absorber electrons to the phonon bath, the standard expression is $\dot{Q} = \Sigma\mathcal{V}(T^5 - T_0^5)$ (Gantmakher, 1974; Roukes *et al.*, 1985; Wellstood, Urbina, and Clarke, 1994; Schwab *et al.*, 2000; Wang *et al.*, 2019), where Σ is a material specific parameter and $\mathcal{V}$ is the volume of the absorber. It is often the case that the temperature difference $\delta T \equiv T - T_0$ is small ($|\delta T/T| \ll 1$), and we can linearize Eq. (10) into

$$\dot{Q} = G_{th}\delta T, \tag{11}$$

where $G_{th} = n\mathcal{K}T_0^{n-1}$ is the thermal conductance between the absorber and the bath. For the previous electron-phonon coupling, we then have $G_{th}^{(ep)} = 5\Sigma\mathcal{V}T_0^4$. We point out that electron-electron relaxation in metals is fast enough to secure a well-defined electron temperature (Pothier *et al.*, 1997).

For the ballistic channel discussed widely in this Colloquium, $G_{th} \equiv G_Q = \pi^2 k_B^2 T_0/(3h)$, and we have for a general temperature difference

$$\dot{Q} = \frac{\pi^2 k_B^2}{6h}(T^2 - T_0^2) = \frac{\pi^2 k_B^2}{3h}T_m\delta T, \tag{12}$$

where $T_m \equiv (T + T_0)/2$ is the mean temperature.

In some experiments a differential two-absorber setup is preferable; see Fig. 2(b). This allows one to measure the temperatures of the two absorbers (T_1 and T_2, separately) and determine the heat flux between the two without extra physical wiring connections for thermometry across the object of interest. In this case equations in this section apply if we replace T and T_0 with T_1 and T_2, respectively. Such a setup offers more flexible calibration and sanity check options for the system, and also for tests of reciprocity (thermal rectification) by inverting the roles of source and drain, i.e., by reversing the temperature bias.

B. Thermometry and temperature control

Here we comment briefly on thermometry and temperature control in the experiments to be reported in this review. The control of the local temperature is typically achieved by Joule heating applied to the electronic system. But depending on the type of reservoir this heat is acting on the quantum conductor

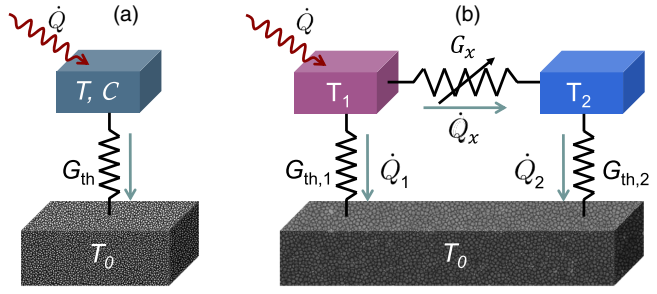

FIG. 2. Thermal models. (a) Finite-sized reservoir at temperature T and of heat capacity $\mathcal{C}$ coupled to a heat bath at fixed temperature T_0 via a heat link with thermal conductance G_{th}. The absorbed heat current $\dot{Q}$ creates a temperature difference. (b) Two finite-sized absorbers coupled to both the heat bath and each other via a potentially tunable thermal conductance G_x with the associated heat current $\dot{Q}_x$ of the system under study.

either directly or indirectly, such as via the phonon bath. The simplest heating element is a resistive on-chip wire.

For heating and local cooling and, in particular, for thermometry, a hybrid normal-metal–insulator–superconductor (*N-I-S*) tunnel junction is a common choice (Giazotto *et al.*, 2006; Muhonen, Meschke, and Pekola, 2012; Courtois *et al.*, 2014). We defer discussion of this technique to Sec. IV.B. In several experiments a simple resistive on-chip wire is used as a local heater. For thermometry one may use a similar wire and measure its thermal noise (Schwab *et al.*, 2000). Another option used in some recent experiments is to measure the current noise of a quantum point contact (Jezouin *et al.*, 2013; Banerjee *et al.*, 2017).

IV. EXPERIMENTAL SETUPS AND BACKGROUND INFORMATION

A. Thermal conductance of a superconductor

A superconductor obeying Bardeen-Cooper-Schrieffer (BCS) theory (Bardeen, Cooper, and Schrieffer, 1957) forms an ideal building block for thermal experiments at low temperatures. A basic feature of a BCS superconductor is its zero resistance, but in our context an even more important property is its essentially vanishing thermal conductance (Bardeen, Rickayzen, and Tewordt, 1959). In bulk superconductors both electronic and nonvanishing lattice thermal conductances play a role.

In small structures the exponentially vanishing thermal conductance at low temperatures can be exploited effectively to form thermal insulators that can at the same time provide perfect electrical contacts. In quantitative terms, according to the theory (Bardeen, Rickayzen, and Tewordt, 1959) the ratio of the thermal conductivity $\kappa_{e,S}$ in the superconducting state and $\kappa_{e,N}$ in the normal state of the same material is given by

$$\kappa_{e,S}/\kappa_{e,N} = \int_{\Delta}^{\infty} d\epsilon \epsilon^2 f'(\epsilon) / \int_{0}^{\infty} d\epsilon \epsilon^2 f'(\epsilon), \tag{13}$$

where $\Delta \approx 1.76 k_B T_C$ is the gap of the superconductor with critical temperature T_C. For temperatures well below T_C, i.e., for $\Delta/(k_B T) \gg 1$, we obtain the following as an approximate answer for Eq. (13):

$$\kappa_{e,S}/\kappa_{e,N} \approx \frac{6}{\pi^2}\left(\frac{\Delta}{k_B T}\right)^2 e^{-\Delta/k_B T}. \tag{14}$$

Since the normal state thermal and electrical conductivities are related by the Wiedemann-Franz law, we obtain

$$\kappa_{e,S} \approx \frac{2\Delta^2}{e^2 \rho T} e^{-\Delta/k_B T}, \tag{15}$$

where ρ is the normal state resistivity of the conductor material. As usual, for the basic case of a uniform conductor with cross-sectional area A and length ℓ we may then associate the thermal conductance G_{th} with thermal conductivity κ as $G_{th} = (A/\ell)\kappa$.

Aluminum and niobium are the most common superconductors used in the experiments described here. In many respects, Al follows BCS theory accurately. In particular, it has been shown (Saira, Kemppinen *et al.*, 2012) that the density of states (DOS) at energies inside the gap is suppressed at least by a factor of $\sim 10^{-7}$ leading to the exponentially high thermal insulation discussed here. The measured thermal conductivity of Al closely follows Eq. (15), as shown by Peltonen *et al.* (2010) and Feshchenko *et al.* (2017). At the same time Nb films suffer from a nonvanishing subgap DOS, leading to power-law thermal conductance in T, i.e., poor thermal insulation in the low temperature regime. In conclusion of this section we emphasize that Al is a perfect thermal insulator at $T \lesssim 0.3 T_C$, except in immediate contact with a normal metal leading to the inverse proximity effect; this proximity induced thermal conductivity typically has an effect only within few hundred nanometers of a clean normal-metal contact (Peltonen *et al.*, 2010).

B. Heat transport in tunneling

One central element of this Colloquium is a tunnel junction between two electrodes L and R. The charge and heat currents through the junction can be obtained using perturbation theory, where the coupling Hamiltonian between the electrodes is written as the tunnel Hamiltonian (Bruus and Flensberg, 2004)

$$\hat{H}_c = \sum_{l,r} (t_{lr} \hat{a}_l^\dagger \hat{a}_r + t_{lr}^* \hat{a}_l \hat{a}_r^\dagger). \tag{16}$$

Here t_{lr} is the tunneling amplitude and $\hat{a}_{l(r)}^\dagger$ and $\hat{a}_{l(r)}$ are the creation and annihilation operators for electrons in the left (right) electrode, respectively.

To have the expression for number current from R to L one first obtains operator for it as $\dot{\hat{N}}_L = (i/\hbar)[\hat{H}_c, \hat{N}_L]$, where $\hat{N}_L = \sum_l \hat{a}_l^\dagger \hat{a}_l$ is the operator for the number of electrons in L. One can then write the charge current operator as $\hat{I} = -e\dot{\hat{N}}_L$. To obtain the expectation value of the current that is measured in an experiment ($I \equiv \langle \hat{I} \rangle$), we employ linear response theory [Kubo formula (Kubo, 1957)] on the corresponding current operator, where $I = -(i/\hbar)\int_{-\infty}^{0} dt' \langle [\hat{I}(0), \hat{H}_c(t')] \rangle_0$, with $\langle \cdot \rangle_0$ the expectation value in the unperturbed state. Assuming that the averages are given by the Fermi distributions in each lead, we have at voltage bias V such that

$$I = \frac{1}{eR_T} \int d\epsilon\, n_L(\tilde{\epsilon}) n_R(\epsilon) [f_L(\tilde{\epsilon}) - f_R(\epsilon)], \tag{17}$$

where $\tilde{\epsilon} = \epsilon - eV$. Here the constant prefactor includes the inverse of the resistance R_T of the junction such that $1/R_T = 2\pi |t|^2 \nu_L(0) \nu_R(0) e^2/\hbar$, with $|t|^2 = |t_{rl}|^2 = \text{const}$ and $\nu_L(0)$ and $\nu_R(0)$ the DOSs in the normal state at Fermi energy in the left and right electrodes, respectively. Under the integral, $n_L(\epsilon)$ and $n_R(\epsilon)$ are the normalized [by $\nu_L(0)$ and $\nu_R(0)$, respectively] energy-dependent DOSs, and $f_L(\epsilon)$ and $f_R(\epsilon)$ are the corresponding energy distributions that are Fermi-Dirac distributions for equilibrium electrodes.

For heat current we use precisely the same procedure but now for the operator of energy of the left electrode

$\hat{H}_{\rm L} = \sum_l \epsilon_l \hat{a}_l^\dagger \hat{a}_l$, instead of the number operator, where ϵ_l is the energy of a single particle state in L. We then determine the expectation value of the heat current from the L electrode ($\dot{Q}_L = -\langle \dot{H}_L \rangle$) as

$$\dot{Q}_{\rm L} = \frac{1}{e^2 R_T} \int d\epsilon\, \tilde{\epsilon} n_{\rm L}(\tilde{\epsilon}) n_{\rm R}(\epsilon)[f_{\rm L}(\tilde{\epsilon}) - f_{\rm R}(\epsilon)]. \quad (18)$$

Here we comment on the relation between the energy and heat currents $\mathcal{J}$ and $\dot{Q}$ introduced in Sec. II. Inserting $\tilde{\epsilon} = \epsilon - eV$, we immediately find that $\dot{Q}_L = \mathcal{J} - IV$, where $\mathcal{J} \equiv (e^2 R_T)^{-1} \int d\epsilon\, \epsilon n_{\rm L}(\tilde{\epsilon}) n_{\rm R}(\epsilon)[f_{\rm L}(\tilde{\epsilon}) - f_{\rm R}(\epsilon)]$. Writing the equation for the heat from the right electrode in analogy with Eq. (18), we find that $\dot{Q}_R = -\mathcal{J}$. Thus, we have $\dot{Q}_L + \dot{Q}_R = -IV$, which presents energy conservation: the total power taken from the source goes into heating the two electrodes. This is natural since in steady state work equals heat, as the internal energy of the system is constant.

As the most basic example of both the electrodes being normal metal [normal-metal–insulator–normal-metal (*N-I-N*) junction], we have $n_{\rm L}(\epsilon) = n_{\rm R}(\epsilon) = 1$. Equations (17) and (18) then yield under relaxed conditions $I = V/R_T$ and $\dot{Q}_{\rm L} = -V^2/(2R_T)$; i.e., the junction is Ohmic and the Joule power is dissipated equally to the two electrodes.

Another important example is a *N-I-S* junction (L = *N*, R = *S*; Fig. 3). Its usefulness in thermometry [see Fig. 3(a)] is based on the superconducting gap Δ that leads to nonlinear, temperature-dependent current-voltage characteristics. This feature probes the temperature of the normal side of the contact. Such a temperature dependence is universal, $d\ln(I/I_0)/dV = e/(k_B T)$, where $I_0 = \sqrt{\pi \Delta k_B T/2}/(eR_T)$, making the *N-I-S* junction a primary thermometer in principle. This is, strictly speaking, true only for an ideal junction with low transparency. Therefore, the common practice is to use it as a secondary thermometer (Lounasmaa, 1974),

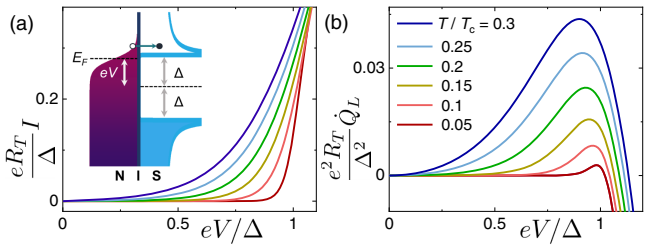

FIG. 3. Properties of a *N-I-S* tunnel junction. (a) Calculated current-voltage curves at different values of $T/T_C = 0.05$–0.3 from bottom to top (both panels). At these subgap voltages the junction provides a sensitive thermometer. Inset: energy diagram of a biased by voltage V junction between a normal-metal (N) and superconducting (S) electrode connected via an insulating (I) barrier. Because of the BCS gap Δ in S, transport is blocked at $eV \ll \Delta$. At a voltage close to the gap value, as in the figure, electrons at the highest energy levels can tunnel to the superconductor as shown, leading to both nonvanishing charge current and cooling of N. (b) Similarly calculated power $\dot{Q}_{\rm L}$ vs V curves, demonstrating cooling of N at $eV \lesssim \Delta$. At higher voltages $eV \gg \Delta$, $\dot{Q}_{\rm L}$ becomes negative, meaning that it serves as a Joule heater of N.

meaning that one measures a thermometric response of it near equilibrium, for instance, the voltage at a small fixed current, against the independently measured temperature of the cryostat (heat bath). The other important feature of the *N-I-S* junction lies in its thermal properties. When biased at a voltage of about Δ/e, heat is carried away from the N side (and the S is heated). That is, it acts as a refrigerator; see Fig. 3(b). At $V \gg \Delta/e$ the junction provides the usual Joule heating. This is how a *N-I-S* junction can be used as both a cooler and a heater of a mesoscopic reservoir. Numerically calculated current-voltage and cooling power characteristics, together with a schematic energy diagram, are depicted in Fig. 3. The main characteristics of a *N-I-S* junction, based on analytical approximations at low temperatures, are $I \approx I_0 e^{-\Delta/k_B T}$ at voltages below the gap, and the maximal cooling of a normal metal at $eV \approx \Delta$ is $\dot{Q}_{\rm L}^{\rm max} \approx +0.59(\Delta^2/e^2 R_T)(k_B T/\Delta)^{3/2}$.

Microrefrigeration by electron transport is a technique that has been reviewed elsewhere (Giazotto *et al.*, 2006; Muhonen, Meschke, and Pekola, 2012; Courtois *et al.*, 2014). References on the topic besides the previously mentioned reviews include Nahum, Eiles, and Martinis (1994), Leivo, Pekola, and Averin (1996), Clark *et al.* (2004), Kuzmin *et al.* (2004), Prance *et al.* (2009), Nguyen *et al.* (2013), and Feshchenko, Koski, and Pekola (2014).

C. Hamiltonian of a quantum circuit

Another key element in our context is a harmonic oscillator, and in some cases a nonlinear quantum oscillator, usually in the form of a Josephson junction (Tinkham, 2004). To avoid dissipation the linear harmonic oscillator in a circuit is commonly made of a superconductor, often in the form of a coplanar wave resonator (Krantz *et al.*, 2019). The Hamiltonian of such an LC oscillator, shown in Fig. 4(a), is composed of the kinetic $q^2/2C$ and potential $\Phi^2/2L$ energies, respectively, where q is the charge on the capacitor and Φ is the flux of the inductor. The charge is the conjugate momentum to flux as $q = C\dot{\Phi}$, and the total Hamiltonian is then

$$\hat{H} = \frac{\hat{q}^2}{2C} + \frac{\hat{\Phi}^2}{2L}, \quad (19)$$

i.e., that of a harmonic oscillator, with $\hat{q}$ and $\hat{\Phi}$ the charge and flux operators, respectively. Introducing the creation $\hat{c}^\dagger$ and annihilation $\hat{c}$ operators such that $[\hat{c}, \hat{c}^\dagger] = 1$, we have

$$\hat{\Phi} = \sqrt{\frac{\hbar Z_0}{2}}(\hat{c} + \hat{c}^\dagger), \qquad \hat{q} = -i\sqrt{\frac{\hbar}{2Z_0}}(\hat{c} - \hat{c}^\dagger), \quad (20)$$

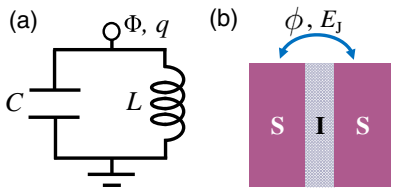

FIG. 4. Central elements of superconducting quantum devices. (a) LC circuit with flux Φ and charge q. (b) Josephson junction with phase difference ϕ and Josephson energy E_J.

which yield the standard harmonic oscillator Hamiltonian

$$H = \hbar\omega_0(\hat{c}^\dagger\hat{c} + \tfrac{1}{2}), \tag{21}$$

where $\omega_0 = 1/\sqrt{LC}$ and $Z_0 = \sqrt{L/C}$ are the angular frequency and impedance of the oscillator.

For a Josephson tunnel junction, shown in Fig. 4(b), the Josephson relations (Josephson, 1962) are

$$\hbar\dot{\phi} = 2eV, \qquad I = I_c \sin\phi, \tag{22}$$

where ϕ is the phase difference across the junction related to flux by $\phi = (2e/\hbar)\Phi$. In the second Josephson relation, I is the current through the junction. The sinusoidal current-phase relation applies strictly to a tunnel junction with critical current I_c. For different types of weak links, sinusoidal dependence does not necessarily hold (Tinkham, 2004). The energy stored in the junction (which is equal to the work done by the source) is then obtained for a current biased case from $I = \partial E/\partial\Phi$ as

$$E = \int^{\Phi} I\, d\Phi = -E_J \cos\phi. \tag{23}$$

Equation (23) constitutes the Josephson part of the Hamiltonian, also called $\hat{H}_J$. For small values of ϕ, ignoring the constant part we have

$$E \simeq \frac{\Phi^2}{2L_J}, \tag{24}$$

where $L_J = \hbar/(2eI_c)$ is the Josephson inductance. Therefore, in the "linear regime" a Josephson junction can be considered a harmonic oscillator such that Eqs. (19)–(21) apply with L replaced by L_J. Yet the actual nonlinearity of a Josephson junction makes it an invaluable component in quantum information processing and in quantum thermodynamics. A magnetic flux tunable Josephson junction, for instance, in the form of two parallel junctions with a superconducting loop in between, is the superconducting quantum interference device (SQUID) discussed in Secs. VII–IX.

D. Quantum noise of a resistor

The quantum noise of a resistor is an important quantity, as it determines the heat emission and absorption in the form of thermal excitations. In Sec. VII it becomes obvious how this noise yields the Joule power in a circuit.

Consider that the resistor in the quantum circuit is formed from a collection of harmonic oscillators with ladder operators $\hat{b}_i$ and $\hat{b}_i^\dagger$ with frequencies ω_i. The phase operator in the interaction picture reads

$$\phi(t) = \sum_i \lambda_i(\hat{b}_i e^{-i\omega_i t} + \hat{b}_i^\dagger e^{i\omega_i t}) \tag{25}$$

with coefficients λ_i. The following voltage fluctuations are related to the phase as $v(t) = (\hbar/e)[\dot{\phi}(t)]$:

$$v(t) = i\frac{\hbar}{e}\sum_i \lambda_i\omega_i(\hat{b}_i^\dagger e^{i\omega_i t} - \hat{b}_i e^{-i\omega_i t}). \tag{26}$$

The spectral density of voltage noise $S_v(\omega) = \int_{-\infty}^{\infty} dt e^{i\omega t}\langle v(t)v(0)\rangle$ is then given by

$$S_v(\omega) = \frac{2\pi\hbar^2}{e^2}\int_0^\infty d\Omega\, \nu(\Omega)\lambda(\Omega)^2\Omega^2\{[1+n(\Omega)]\delta(\omega-\Omega) + n(\Omega)\delta(\omega+\Omega)\}, \tag{27}$$

where $\nu(\Omega)$ is the oscillator density of states. Now we consider both positive and negative frequencies, which correspond to the quantum emission and absorption processes. For positive frequencies only the first term survives as

$$S_v(\omega) = \frac{2\pi\hbar^2}{e^2}\nu(\omega)\lambda(\omega)\omega^2[1+n(\omega)]. \tag{28}$$

Similarly considering the negative frequencies, we find that

$$S_v(-\omega) = e^{-\beta\hbar\omega}S_v(\omega), \tag{29}$$

which is the *detailed balance condition*.

We know that the classical Johnson-Nyquist noise (Johnson, 1928; Nyquist, 1928) of a resistor at $k_BT \gg \hbar\omega$ reads

$$S_v(\omega) = 2k_BTR. \tag{30}$$

This is the classical fluctuation-dissipation theorem (FDT) (Callen and Welton, 1951) applied to the resistor. In this limit, by using the Taylor expansion we have $(1-e^{-\beta\hbar\omega})^{-1} \simeq (\beta\hbar\omega)^{-1}$, so using Eq. (28) we have the following connection between the oscillator properties and the physical resistance (Karimi and Pekola, 2021):

$$\lambda_i^2 = \frac{Re^2}{\pi\hbar\nu(\omega_i)\omega_i}. \tag{31}$$

Substituting this result into Eq. (27), we obtain at all frequencies

$$S_v(\omega) = 2R\frac{\hbar\omega}{1-e^{-\beta\hbar\omega}}. \tag{32}$$

V. PHONONS

Quantized thermal conductance was demonstrated experimentally for the first time by Schwab *et al.* (2000). In their setup, as shown in the inset of Fig. 5, the "phonon cavity" consists of a 4×4 μm^2 block of a silicon nitride membrane with 60 nm thickness suspended by four legs of equal thickness. Each leg has catenoid waveguide shape whose diameter at the narrowest point is less than 200 nm. This waveguide shape as a 1D channel is the ideal profile to achieve unit transmissivity between the suspended cavity and the bulk reservoir (Rego and Kirczenow, 1998). Two Au-film resistors with 25 nm thickness were patterned on the suspended central

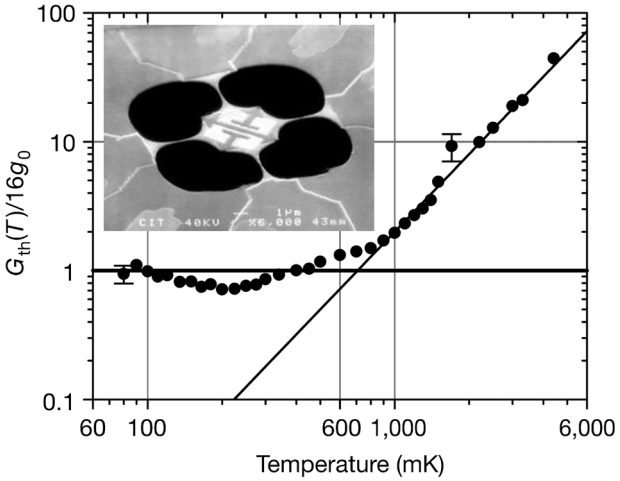

FIG. 5. View of the suspended structure of Schwab *et al.* (2000) for measuring quantized thermal conductance. Main panel: temperature dependence of the measured thermal conductance normalized by $16G_Q$ $(16g_0)$. Inset: in the center, a 4×4 μm^2 phonon cavity is patterned from the membrane; the bright areas on the central membrane are Au-thin-film transducers connected to Nb-thin-film leads on top of phonon waveguides. The membrane has been completely removed in the dark regions. Adapted from Schwab *et al.*, 2000.

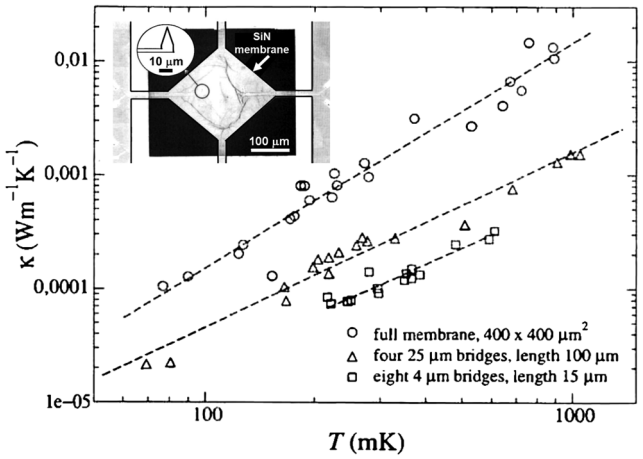

FIG. 6. Thermal conductivity κ of a 200-nm-thick silicon nitride membrane measured in three different geometries as a function of membrane temperature. Dashed lines present the fitted functions: $\kappa \simeq 14.5T^{1.98}$ mW m^{-1} K^{-1} for the full membrane and $\kappa \simeq 1.58T^{1.54}$ and $0.57T^{1.37}$ mW m^{-1} K^{-1} for 25- and 4-μm-wide bridges, respectively, where T is expressed in kelvins. The data for a 400×400 μm^2 full membrane and a 25-μm-wide bridge were presented by Leivo and Pekola (1998), while those for a 4-μm-wide bridge are unpublished (Leivo, 1999). The corresponding thermal conductance $G_{th} = \kappa A/L$ for one bridge with area A and length L at $T = 0.1$ K for both 25 and 4 μm are 2.3×10^{-12} and 1.3×10^{-12} W/K, which give $N \simeq 24$ and 14, respectively, assuming fully ballistic channels. Adapted from Leivo and Pekola, 1998, and Leivo, 1999.

block; one of them serves to apply the Joule heating to generate the temperature gradient along the legs, and the other one worked as a thermometer to measure the phonon cavity temperature. The electron temperature of the resistor was measured with a low noise amplifier (dc SQUID) operating with nearly quantum-limited energy sensitivity by measuring the electrical Johnson noise of the resistor.

The measurement of Schwab *et al.* (2000) probes the thermal conductance by phonons across the four silicon nitride bridges as a function of bath temperature. These data are shown in the main panel of Fig. 5. The result exhibits the usual phononic thermal conductance ($\propto T^3$) at temperatures above 1 K. Below this temperature there is a rather abrupt leveling off of G_{th} to the value $16G_Q$ (here the notation is such that $g_0 \equiv G_Q$). Schwab *et al.* (2000) argue that the coefficient 16 arises from the trivial factor 4 due to four independent bridges in the structure and the less trivial factor 4 due to four possible acoustic vibration modes of each leg in the low temperature limit: one longitudinal, one torsional, and two transverse modes. In later theoretical works the somewhat meandering behavior of G_{th}/G_Q below the crossover temperature was explained to arise from the remaining scattering of phonons in the bridges, i.e., from nonballistic transport, whose effect is expected to get weaker in the low temperature limit (Santamore and Cross, 2001).

Over the years, there have been a few other experiments on thermal conductance by phonons in restricted geometries. The one by Leivo (Manninen, Leivo, and Pekola, 1997; Leivo and Pekola, 1998; Leivo, 1999) employed 200-nm-thick silicon nitride membranes in various geometries; see Fig. 6. The experiments were performed by applying Joule heating on a central membrane in a manner analogous to the experiment of Schwab *et al.* (2000), and the resulting temperature change to obtain the thermal conductance was then read out by measuring the temperature-dependent conductance of *N-I-S* probes processed on top of the same membrane. In this case the wiring running along the bridges was made of aluminum, which is known to provide close to perfect thermal isolation at temperatures well below the superconducting transition at $T_C \approx 1.4$ K; see Sec. IV.A. In general, there are many conduction channels in the wide bridges, as demonstrated in the Fig. 6 caption. Yet this number for a single $w = 4$ μm wide bridge is $N = 14$ at $T = 100$ mK, which is already close to the prediction of $N = 4$ given by Rego and Kirczenow (1998). The ballisticity of these 15 μm long bridges is unknown, though. Yet these experiments provide evidence of thermal conductance close to the quantum limit.

The experiment of Schwab *et al.* (2000) was followed by several measurements using different temperature ranges and materials. Experiments on GaAs phonon bridges of sub-μm lateral dimensions were previously performed at temperatures above 1 K (Tighe, Worlock, and Roukes, 1997) and later down to 25 mK bath temperature (Yung, Schmidt, and Cleland, 2002). The latter experiment measuring the temperature of the GaAs platform in the middle using *N-I-S* tunnel junctions demonstrated Debye thermal conductance at $T \gg 100$ mK but tended to follow the expected quantum thermal conductance at the lowest temperatures. In the more recent experiments by Tavakoli *et al.* (2017, 2018) the measurement on submicronwide silicon nitride bridges was made differential in the sense that there was no need to add superconducting leads on these phonon-conducting legs. The results at the lowest

temperatures of ∼0.1 K fall about 1 order of magnitude below the quantum value, and the temperature dependence of thermal conductance is close to T^2. Tavakoli *et al.* (2017, 2018) proposed nonballistic transmission in their bridges as the origin of their results. Finally, experiments by Zen *et al.* (2014) demonstrated that thermal conductance can be strongly suppressed even in two dimensions with proper patterning of the membranes into a nanostructured periodic phononic crystal.

VI. ELECTRONS AND FRACTIONAL CHARGES

Charged particles play a special role in assessing quantum transport properties since they provide straightforward access to both the particle number current and the heat current. For instance, in the case of electrons we can count the carriers by directly measuring the charge current and the associated conductance. When the mean free path of the carriers is much larger than the physical dimensions of the contact, transport can become ballistic. According to Eq. (4), the electrical conductance then assumes only integer multiple values of elementary conductance quantum. The first experiments on quantized conductance of a point contact in a GaAs-AlGaAs two-dimensional high mobility electron gas (2DEG) heterostructures were performed by van Wees *et al.* (1988) and Wharam *et al.* (1988). van Wees *et al.* (1988) formed the point contact using a top metallic gate with a width $W \simeq 250$ nm opening in a tapered geometry to form a voltage-controlled narrow and short channel in the underlying electron gas. The layout of the gate electrode is shown in the inset of Fig. 7. At negative gate voltages electrons are repelled under the gate and the width of the channel for carriers is $\lesssim$100 nm, which is well below the mean free path of $l \simeq 8.5$ μm. The measured conductance of the point contact shown in Fig. 7 exhibits well-defined plateaus at the expected positions $N2e^2/h$ as a function of applied gate voltage (van Wees *et al.*, 1988). The factor of 2 with respect to Eq. (4) arises from spin degeneracy.

Thirty years after the experiments on quantized electrical conductance by electrons (van Wees *et al.*, 1988; Wharam *et al.*, 1988), Jezouin *et al.* (2013) measured the quantum-limited heat conductance of electrons in a quantum point contact. The principle and practical implementation of this

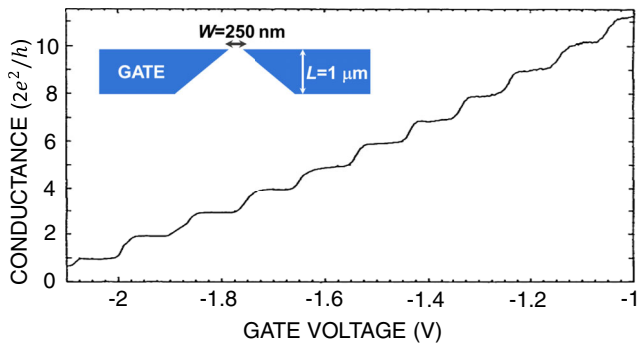

FIG. 7. Measured quantized conductance of a point contact in a two-dimensional electron gas as a function of gate voltage. The conductance demonstrates plateaus at multiples of $2e^2/h$. Inset: schematic layout of the point contact. Adapted from van Wees *et al.*, 1988.

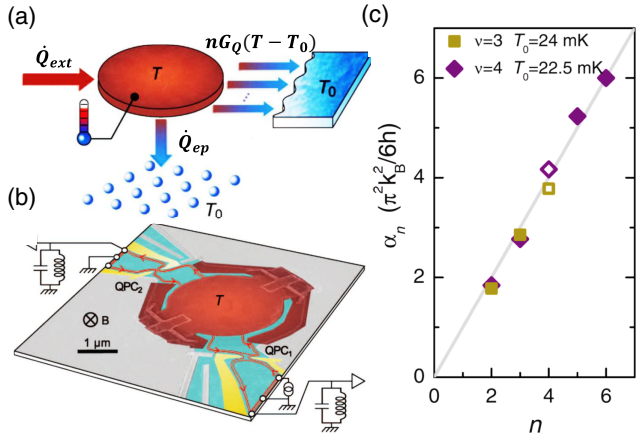

FIG. 8. Measuring quantized heat carried by electrons. (a) When Joule power $\dot{Q}_{\rm ext}$ is applied to a metal plate (brown disk), the electronic temperature increases up to T, and the heat then flows via n ballistic quantum channels to the reservoir and the phonon heat bath $\dot{Q}_{\rm ep}$, which both have fixed temperature T_0. (b) Colored scanning electron micrograph of the measured sample. In the center, the metallic Ohmic contact in brown is connected to two quantum point contacts ($\rm QPC_1$ and $\rm QPC_2$) in yellow (lightest area) via a two-dimensional Ga(Al)As electron gas in light green (surrounding the point contacts). The red lines with arrows around the metal plate indicate the two propagating edge channels ($\nu = 3$ or 4). The Joule power is applied to the metallic plate through a QPC, and the two LC-tank circuits are for noise thermometry measurements. (c) The gray line shows the predictions for the quantum limit of the heat flow, while the symbols exhibit the extracted electronic heat current normalized by $\pi^2k_B^2/(6h)$ as a function of the number of electronic channels n. Adapted from Jezouin *et al.*, 2013.

experiment and its setup are shown in Figs. 8(a) and 8(b). A micrometer-sized metal plate is connected to both a cold phonon bath and a large electronic reservoir via an adjustable number n of ballistic quantum channels with both reservoirs at T_0, as shown in Fig. 8(a). By injecting Joule power $\dot{Q}_{\rm ext}$ to the metallic plate, the electrons were heated up to temperature T, which can be directly measured by a noise thermometer. This power is then transmitted via the n quantum channels at the rate $nG_{\rm Q}(T - T_0)$ through two quantum point contacts ($\rm QPC_1$ and $\rm QPC_2$) and to the phonon bath at rate $\dot{Q}_{\rm ep}$, which is independent of n. The two QPCs display clear plateaus of the measured electrical conductance at n_1e^2/h and n_2e^2/h, respectively, where n_1 and n_2 are integers. The sum $n = n_1 + n_2$ determines the number of quanta carrying the heat out of the plate electronically. The structure used in this experiment (Jezouin *et al.*, 2013) satisfies the conditions of having sufficient electrical and thermal contact between the metal plate and the two-dimensional electron gas underneath. Moreover, the thermal coupling to the phonon bath and via the QPCs is weak enough that the central electronic system forms a uniform Fermi gas (fast electron-electron relaxation and diffusion across the plate) at temperature T. A perpendicular magnetic field was applied to the sample so as to be in the integer quantum Hall effect regime at filling factors $\nu = 3$ or 4. Figure 8(c) shows α_n, the measured electronic heat conductance normalized by $\pi^2k_B^2/(6h)$ as a

function of the number n of electronic channels as symbols that fall on a straight line with unit slope shown by the gray line, thus demonstrating the quantized thermal conductance at the expected level. Equivalently, this experiment demonstrates Wiedemann-Franz law on the current plateaus.

The work of Jezouin *et al.* (2013) was preceeded by two experiments of some two decades earlier (Molenkamp *et al.*, 1992; Chiatti *et al.*, 2006), where G_Q was tested with an order of magnitude accuracy. Both measurements were performed on GaAs-based 2DEGs, and in both of them, thermal conductance was obtained by measuring the Seebeck coefficient (thermopower) and extracting the corresponding temperature difference. Molenkamp *et al.* (1992) then determined G_{th}, which agrees within a factor of 2 with the assumption that the Wiedemann-Franz law applies to the conduction plateaus of the QPC. Chiatti *et al.* (2006) conducted a similar experiment with the same philosophy but with improved control of the structure and system parameters. With these assumptions there is good agreement between thermal conductance and electrical conductance via the Wiedemann-Franz law.

In recent years, it has become possible to measure quantized thermal conductance even at room temperature (Cui *et al.*, 2017; Mosso *et al.*, 2017). The experiments are performed on metallic contacts of atomic size with scanning thermal microscopy probes. The material of choice is typically Au, although experiments on Pt have also been reported (Cui *et al.*, 2017). The setup and experimental observations of Cui *et al.* (2017) are presented in Fig. 9. The electrical conductance plateaus at multiples of $2e^2/h$ are typically seen when pulling the contact to the few conductance channel limit. The noteworthy feature in the data is that the simultaneous thermometric measurement confirms the Wiedemann-Franz law for electric transport within 5%–10% accuracy, thereby demonstrating quantized thermal conductance (Cui *et al.*, 2017).

In the measurement performed by Banerjee *et al.* (2017), the value of the quantum of thermal conductance for different Hall states including integer and fractional states was verified. They first confirmed the observations of Jezouin *et al.* (2013) in a similar setup in the integer states with filling factors $\nu = 1$ and 2. Figure 10(a) demonstrates the validity of quantized heat conductance at $\Delta N G_Q$ for $\Delta N = 1, 2, \ldots, 6$ channels with about 3% accuracy (inset). The main result of the work is the observation of thermal conductance of strongly interacting fractional states. Figure 10(b) shows that the thermal conductance is again a multiple of G_Q, even for the (particlelike) $\nu = 1/3$ fractional state, although the electrical conductance is normalized by the effective charge $e^* = e/3$. As a whole, the work covers both particlelike and holelike fractional states, testing the predictions of Kane and Fisher (1997).

As a final point in this section we mention that there are a large number of further experiments on various heat transport effects performed in the quantum Hall regime. We do not cover these experiments in detail here; see Granger, Eisenstein, and Reno (2009), Altimiras *et al.* (2010), le Sueur (2010), Nam, Hwang, and Lee (2013), Halbertal *et al.* (2016, 2017), Banerjee *et al.* (2018), Sivre *et al.* (2018), and Srivastav *et al.* (2019).

VII. PHOTONS

In this section we discuss transport by thermal microwave photons, presenting another bosonic system to study in this context.

A. A ballistic photon channel

The concept of microwave photon heat transport becomes concrete when it is described on a circuit level (Schmidt,

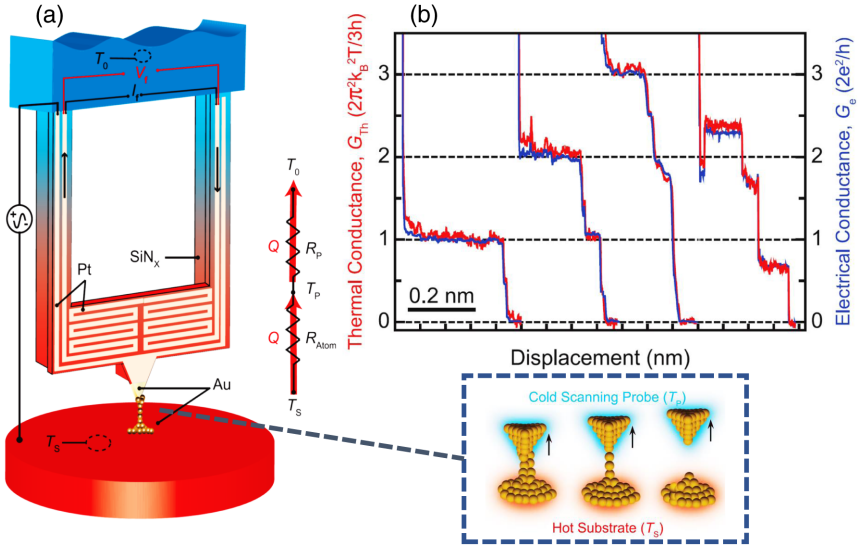

FIG. 9. Experimental setup and results on quantized thermal conductance in single atom junctions. (a) Calorimetric scanning thermal microscopy probe that schematically shows how to connect atomic junctions to a heated metallic substrate. By applying a small voltage bias and measuring the resulting current, the electrical conductance of the tip-substrate junction can be measured. T_S and T_0 are the temperatures of the substrate and the thermal reservoir, respectively. The enlargement schematically depicts the atomic chains forming, narrowing, and breaking during the withdrawal of the probe from the heated substrate. (b) Almost overlapping measured thermal (red, left) and electrical (blue, right) conductance traces normalized by $2\pi^2k_B^2T/(3h)$ and $2e^2/h$, respectively. Adapted from Cui *et al.*, 2017.

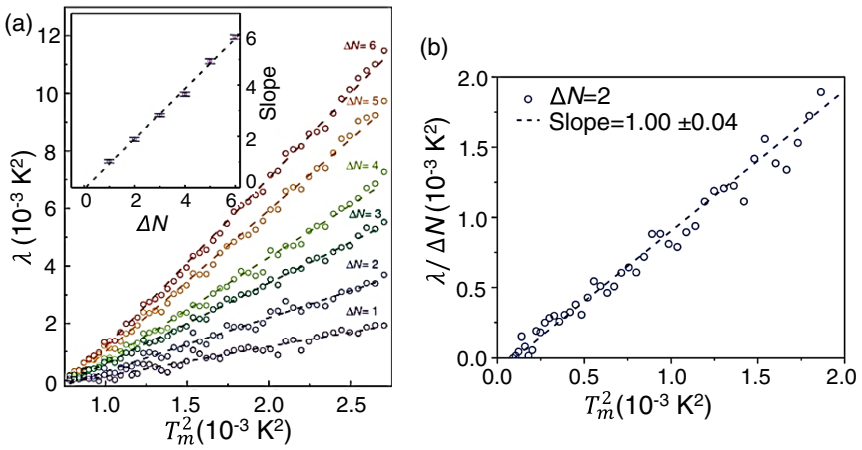

FIG. 10. Measurements in the (a) integer and (b) fractional quantum Hall regimes with filling factors $\nu = 2$ and $1/3$, respectively. (a) Normalized coefficient of the dissipated power $\lambda = \delta P/(G_Q/2T)$ as a function of T_m^2 for different configurations of $\Delta N = N_i - N_j$, where N is the number of channels. The difference is presented in order to eliminate the N-independent contribution of the phononic heat current. Here δP is the difference between dissipated power at different N, $\delta P = \Delta P(N_i, T_m) - \Delta P(N_j, T_m)$, and T_m is the calculated temperature of the floating contact. The circles show the measured data and the dashed lines are linear fits to them. The slope of each set is shown in the inset as a function of ΔN. The linear dependence has approximately unit slope (0.98 ± 0.03), confirming the quantum of thermal conductance for this integer state ($\nu = 2$). (b) Case of the fractional state $\nu = 1/3$. It is the same as (a) except that here the difference of λ between $N = 4$ and 2 is normalized by ΔN as a function of T_m^2. The slope of the linear fit (dashed line) to the measured data (circles) is close to unity. Adapted from Banerjee *et al.*, 2017.

Schoelkopf, and Cleland, 2004). We start with a setup familiar from the century-old discussion by Johnson (1928) and Nyquist (1928). Two resistors R_1 and R_2 are directly coupled there to each other as shown in Fig. 11(a). They are generally at different temperatures T_1 and T_2. Each resistor then produces thermal noise with the spectrum $S_v(\omega)$ of Eq. (32); i.e., they are thermal photon sources. We first consider the fact that R_1 generates noise current i_1 on resistor R_2 as $i_1 = v_1/(R_1 + R_2)$. The spectral density of current noise is then $S_{i_1}(\omega) = (R_1 + R_2)^{-2} S_{v_1}(\omega)$. The voltage noise produced by resistor

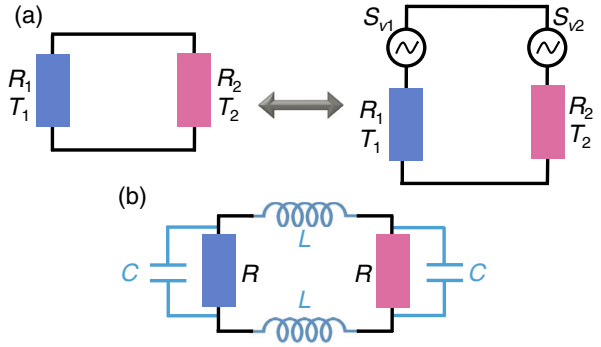

FIG. 11. Setup of two resistors R_1 and R_2 at temperatures T_1 and T_2, respectively, interacting with each other via the respective thermal noises. We present the quantum version of the classical Johnson-Nyquist problem in the text with the associated radiative heat current. (a) The plain two-resistor heat exchange can be modeled using a circuit approach where each resistor is accompanied by a thermal voltage noise source. The two sources are uncorrelated. (b) A realistic circuit includes inevitably reactive elements as well, as discussed in the text. These are added in the figure to allow for an analysis of the crossover between the quantum and classical regimes upon varying the operating temperature and the physical system size.

R_i $(i = 1, 2)$ is $S_{v_i}(\omega) = 2R_i\hbar\omega/(1 - e^{-\beta_i\hbar\omega})$ for $i = 1, 2$. The power density produced by the noise of R_1 and dissipated in resistor R_2 is then $S_{P_2}(\omega) = [R_2/(R_1 + R_2)^2] S_{v_1}(\omega)$. The corresponding total power dissipated in resistor R_2 due to the noise of resistor R_1 is

$$P_2 = \int_{-\infty}^{\infty} \frac{d\omega}{2\pi} S_{P_2}(\omega) = \frac{4R_1R_2}{(R_1 + R_2)^2} \int_0^{\infty} \frac{d\omega}{2\pi} \hbar\omega \left[n_1(\omega) + \frac{1}{2} \right]. \tag{33}$$

The net heat flux from 1 to 2 (P_{net}) is the difference between P_2 and P_1, where P_1 is the corresponding power produced by R_2 on R_1 by the uncorrelated voltage (current) noise described similarly. Thus,

$$P_{\text{net}} = \frac{4R_1R_2}{(R_1 + R_2)^2} \frac{\pi k_B^2}{12\hbar} (T_1^2 - T_2^2). \tag{34}$$

Note that the integrals for P_1 and P_2 separately [see Eq. (33)] would lead to a divergence due to the zero point fluctuation term, but since these fluctuations cannot transport energy this term cancels out in the physical net power [Eq. (34)]. We find that, for a small temperature difference with $T_1 = T_2 \equiv T$,

$$G_\nu = \left. \frac{dP_{\text{net}}}{dT_1} \right|_T = \frac{4R_1R_2}{(R_1 + R_2)^2} \frac{\pi k_B^2}{6\hbar} T, \tag{35}$$

which is equal to the quantum of heat conductance

$$G_\nu = G_Q \tag{36}$$

for $R_1 = R_2$. For a general combination of resistance values the factor

$$r = \frac{4R_1R_2}{(R_1+R_2)^2} \tag{37}$$

represents a transmission coefficient. The circuit model for heat transport can be generalized to essentially any linear circuit composed of reactive elements and resistors, as was done by Pascal, Courtois, and Hekking (2011) and Thomas, Pekola, and Golubev (2019).

B. Circuit limitations of the ballistic picture

What are the physical conditions for the experiment in a circuit to yield thermal conductance that is governed by G_Q? The Johnson-Nyquist work (Johnson, 1928; Nyquist, 1928) was out of this domain, as was a more recent experiment by Ciliberto *et al.* (2013). The necessary key ingredients for "quantumness" are that the experiment combines low temperatures and physically small structures. More quantitatively, the realistic circuit is never presented fully by the simple combination of two resistors, but the full picture of it instead also includes inevitable reactive elements. A way of describing a more realistic circuit (Golubev and Pekola, 2015) is to include a parallel capacitance and series inductance in the basic circuit, as shown in Fig. 11(b). The point is that electromagnetics tells us that an order of magnitude estimate for capacitance is given by $C \sim \epsilon\ell$ and inductance by $L \sim \mu_0\ell$, where ℓ is the overall linear dimension of the circuit and ϵ and μ_0 are the permittivity and permeability of the medium. To observe the pure quantum thermal conductance, one needs to have a ballistic channel between the resistor baths, which in this case means that the series inductor presents a small impedance and the parallel capacitance presents a large impedance. These both are to be compared to the resistances in the circuit at all relevant frequencies, meaning up to $\omega_{th} = k_BT/\hbar$, the thermal cutoff of the resistor at temperature T. In form of simple inequalities we then need to require $\omega_{th}L \ll R \ll (\omega_{th}C)^{-1}$, and based on our previous arguments this transforms into

$$\epsilon\ell k_BTR/\hbar \ll 1, \qquad \mu_0\ell k_BT/(\hbar R) \ll 1. \tag{38}$$

It is now easy to verify the statements at the beginning of this section. We assume for simplicity a typical value for a resistance used in some experiments ($R = 100\ \Omega$). If we take a mesoscopic circuit with $\ell = 100\ \mu$m at a low temperature $T = 100$ mK, we find that $\epsilon\ell k_BTR/\hbar \approx \mu_0\ell k_BT/(\hbar R) \approx 0.01$, which satisfies the conditions in Eqs. (38). On the other hand, an $\ell = 0.1$ m macroscopic circuit at room temperature ($T = 300$ K) yields $\epsilon\ell k_BTR/\hbar \approx \mu_0\ell k_BT/(\hbar R) \approx 3\times10^4$, which is far into the classical regime. Some of those conditions can be avoided in a low temperature transmission line circuit (Partanen *et al.*, 2016), as we discuss later.

C. Experiments on heat mediated by microwave photons

We modeled in Sec. VII the heat emitted by a resistor and absorbed by another one in an otherwise dissipationless circuit. It was shown (Schmidt, Schoelkopf, and Cleland, 2004) that this heat carried by microwave photons behaves as if the two resistors were coupled by a contact whose ballisticity is controlled by the impedances in the circuit. Ideally, two physically small and identical resistors at low temperatures can come close to the ballistic limit, with thermal conductance approaching G_Q. Motivated by this observation, several experiments assessing this result were set up in the past two decades (Meschke, Guichard, and Pekola, 2006; Timofeev *et al.*, 2009; Partanen *et al.*, 2016). They were all performed essentially in the same scenario: the resistors are normal metallic thin-film strips with sufficiently small size that their temperature varies significantly in response to typical changes of power affecting them. The electrical connection between the resistors is provided by superconducting aluminum leads, whose electronic heat conductance is vanishingly small at the temperature of operation; see Sec. IV.A. In one of the experiments (Meschke, Guichard, and Pekola, 2006) the superconducting lines were interrupted by a SQUID that acts as a tunable inductor providing a magnetic-flux-controlled valve of photon mediated heat current. All these experiments were performed at $T \sim 0.1$ K, far below $T_C \approx 1.4$ K of aluminum. Temperatures are controlled and monitored by biased *N-I-S* tunnel junctions.

The experiment of Timofeev *et al.* (2009) was designed to mimic as closely as possible the basic configuration of Fig. 11(a) with a superconducting Al loop. In this case the distance between the resistors was about 50 μm, and the temperatures of both the heated (or cooled) source and the drain resistor were measured. The experiment [Figs. 12(a)–12(c)] demonstrates thermal transport via the electronic channel, i.e., the quasiparticle thermal transport (Bardeen, Rickayzen, and Tewordt, 1959) described in Sec. IV.A, at temperatures exceeding ~250 mK. The result in this regime is in line with the basic theory, given the dimensions and material parameters of the aluminum leads. Below about 200 mK the photon contribution kicks in. In the loop geometry it turns out that the temperatures of the two resistors follow each other closely at the lowest bath temperatures, yielding thermal conductance given by G_Q. Some uncertainty remains about the absolute value of G_ν since the precise magnitude of the competing electron-phonon heat transport coefficient Σ remained somewhat uncertain. The measurement was backed by a reference experiment, where a sample similar to that described previously was measured under the same conditions and fabricated in the same way. This reference sample intentionally lacked one arm of the loop leading to poor matching of the circuit in the spirit discussed in Sec. VII.B. In this case the quasiparticle heat transport prevails as in the matched sample, but the photon G_ν is vanishingly small, confirming, one could say even quantitatively, the ideas presented about the heat transfer via a nonvanishing reactive impedance.

The previously described experiment was performed on a structure with physical dimensions not exceeding 100 μm. A natural question arises: is it possible to transport heat over macroscopic distances by microwave photons, like radiating the heat away from the entire chip? This could be important in quantum information applications; for superconducting qubit realizations, see Kjaergaard *et al.* (2020). This question was addressed experimentally by Partanen *et al.* (2016)

[Figs. 12(d) and 12(e)], who placed the two resistors at a distance of about 10 mm, i.e., about 100 times farther away from each other than was done earlier. Furthermore, the connecting line between the two baths was a 1 m long meander made of a superconductor, which acted as a transmission line. Such a coplanar line typically has an impedance of about 50 Ω irrespective of its length, thus potentially supporting the heat transport even over large distances. The thermal conductance was measured as in the work of Timofeev *et al.* (2009), with similar results proving the hypothesis of photon transport over macroscopic distances. These experiments may open the way for practical heat transport schemes in microwave circuits.

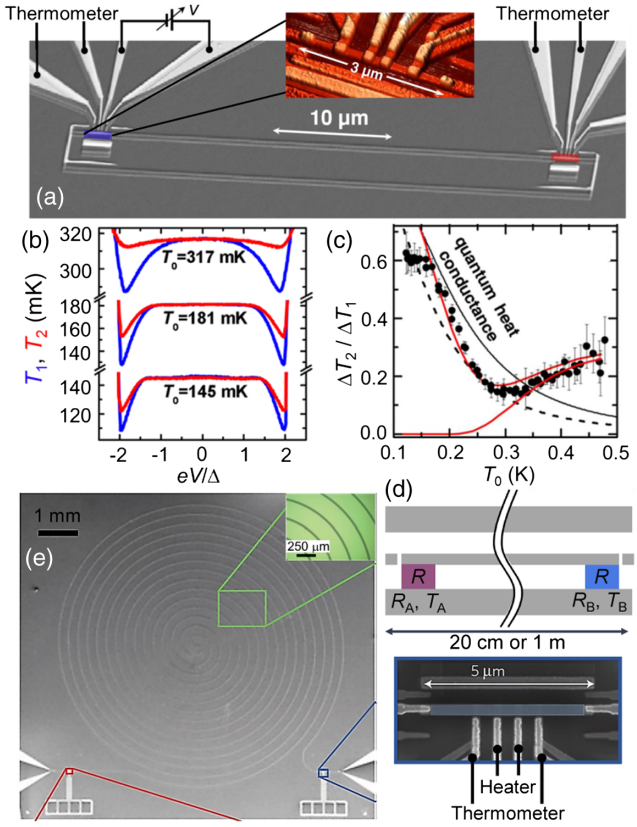

FIG. 12. Quantum-limited heat conduction over microscopic and macroscopic distances. (a) The scanning electron micrograph (SEM) of two AuPd resistors at a distance of 50 μm are connected via Al superconducting lines into a loop to match the impedance between them to reach the full quantum of heat conductance. *N-I-S* probe junctions are used to apply Joule heat and to measure the island temperature. (b) Measured local island temperature T_1 (blue) and remote one T_2 (red) as functions of applied bias voltage on a *N-I-S* junction pair at different bath temperatures T_0. The drop for T_1 is naturally stronger than that for T_2. (c) Measured relative temperature drops (symbols) $\Delta T_2/\Delta T_1$ against T_0 at the optimum cooling bias voltage obtained from data like those in (b). The descending solid and dashed black lines are obtained from the linearized thermal model, which is simply given by $\Delta T_2/\Delta T_1 = G_x/(G_x + G_{\mathrm{th},2})$ [see Fig. 2(b)] at low temperatures. The thermal model is that shown in Fig. 2(b). The electron-phonon constant is considered to be $\Sigma_{\mathrm{AuPd}} = 2 \times 10^9$ and 4×10^9 W K^{-5} m^{-3} for the solid and dashed lines, respectively. The remaining red solid lines are the results of the numerical thermal model. (a)–(c) Adapted from Timofeev *et al.*, 2009. (d) Superconducting transmission line terminated at the two ends by normal-metal resistances R_A and R_B at two different electron temperatures T_A and T_B, respectively. (e) SEM image of an actual device, where the length of the coplanar waveguide (transmission line), made out of Al, is either 20 cm or 1 m and has a double-spiral structure. An enlarged SEM image of one of the resistors (made out of either AuPd or Cu) with a simplified measurement scheme is shown in the bottom right of the panel. (d),(e) Adapted from Partanen *et al.*, 2016.

VIII. TUNABLE QUANTUM HEAT TRANSPORT

In this section we describe quantum systems where heat transport is controlled by either the magnetic or electric field

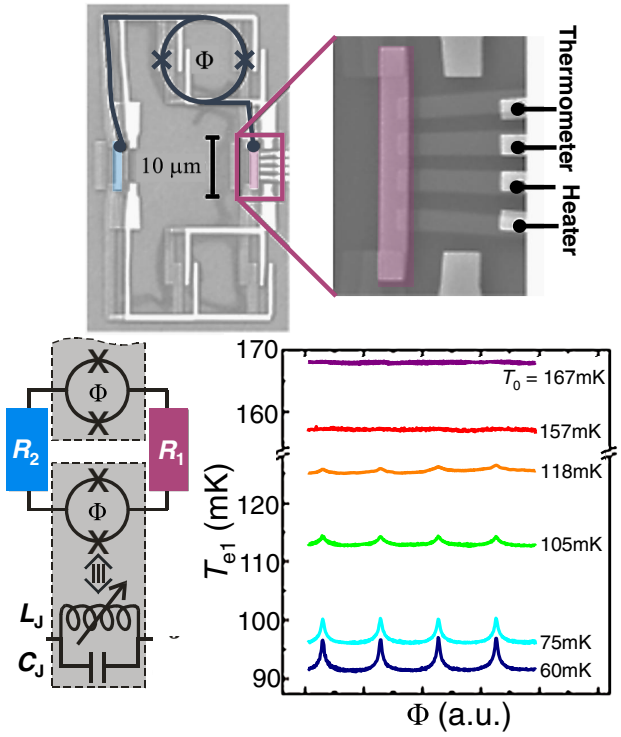

FIG. 13. Photon thermal transport controlled by magnetic flux. Top left panel: SEM of the device, where two nominally identical normal-metal resistors R_1 and R_2 (colored in blue and red on the left and right, respectively), made out of AuPd, are connected to each other via two aluminum superconducting leads, interrupted by a dc SQUID (a superconducting loop with two Josephson junctions indicated by the cross sign) in each line. The SQUIDs again serve as thermal switches between the resistors and can be controlled by external magnetic flux Φ. Top right panel: magnified view of R_1, which is connected to four *N-I-S* tunnel junctions to the right and two *N-S* contacts at the top and bottom to allow thermometry and Joule heating. Bottom left panel: schematic illustration of the electrical model of the actual sample. Bottom right panel: measured flux modulation of the electron temperature T_{e1} in R_1 as a function of applied magnetic flux Φ for different values of the bath temperature T_0. The modulation decreases monotonically by increasing T_0 because of stronger coupling to the phonon bath. The maxima in T_{e1} correspond to the weakest electron-photon coupling at half-integer values of Φ/Φ_0, where $\Phi_0 = h/(2e)$ is the magnetic flux quantum. Adapted from Meschke, Guichard, and Pekola, 2006.

to achieve useful functional operation. These devices include heat valves, heat interferometers, thermal rectifiers, and circuit refrigerators. Mesoscopic structures provide an option for controlling currents using external fields. Concerning charge currents, SQUIDs (Tinkham, 2004) and single-electron transistors (Averin and Likharev, 1991) provide hallmark devices in this context, where the magnetic field (flux in a superconducting loop) and electric field (gate voltage), respectively, are the parameters that control the current.

The first experiment on heat transport by thermal microwave photons (Meschke, Guichard, and Pekola, 2006) was realized in a setup where a SQUID was used as a heat valve. The experiment depicted in Fig. 13 shows two metallic AuPd resistors at a distance of a few tens of micrometers from each other, connected by superconducting Al lines. The loop is interrupted in each arm by a SQUID, whose flux can be controlled by the common external field for both of them. The thermal model of Fig. 2(b) applies to this circuit. In the experiment only the heated resistor's temperature T_{e1} was measured. The panel on the bottom right of Fig. 13 displays the magnetic-flux-dependent variation of temperature T_{e1} at different bath temperatures T_0 under a constant level of heating. At bath temperatures well above 100 mK, the flux dependence vanishes since the inter-resistance thermal conductance by photons $\propto T$ is much weaker than the conductance to the phonon bath $\propto T^4$. On the contrary, toward low temperatures below 100 mK, the electron temperature T_{e1} varies with magnetic flux as the inter-resistor coupling becomes comparable to the bath coupling, demonstrating the photonic thermal conductance. Moreover, the magnitude of the thermal conductance was shown to quantitatively follow from the circuit model presented in Sec. III.A when applied to the current setup. Among other things, the data and this calculation predicted that at $T_0 = 60$ mK the maximum value of thermal conductance with zero flux in the SQUID (i.e., with minimum Josephson inductance) was ~50% of G_Q.

The photonic heat current was controlled by the magnetic field in the previous example. A dual method is to apply the electric field as a control, as indicated in Fig. 14(a). This procedure was realized in a recent experiment (Maillet *et al.*, 2020), where the superconducting loop is interrupted by a Cooper-pair transistor ["charge qubit" (Nakamura, Pashkin, and Tsai (1999)]. In this setup, the Josephson coupling is tuned by the gate voltage. The thermal model of the experiment is pretty much as before, except that the Josephson element with its control field is different. In general it is easier to apply the electric field using gate voltage, especially locally on the chip, than local magnetic flux. As shown in Fig. 14(a), the device demonstrates gate-dependent modulation of the heat current. Its overall magnitude is consistent with the modeling of the circuit: at maximum thermal conductance $G_\nu \approx 0.35 G_Q$ was achieved.

As to the heat currents in single-electron circuits, similar control principles apply in general. An early experiment to control heat flow using gate voltage in a single-electron transistor formed of *N-I-S* junctions was performed by Saira *et al.* (2007). The results on temperature of the system were quantitatively confirmed by a model employing standard single-electron tunneling theory and a heat balance equation on the measured central island of the transistor. Heat transport via a fully normal metallic single-electron transistor was measured by Dutta *et al.* (2017). Results of this experiment are shown in Fig. 14(b). The heat current between the source and drain with a temperature bias applied across was carried by electrons and modulated by the gate voltage such that the observed thermal conductance and simultaneously measured

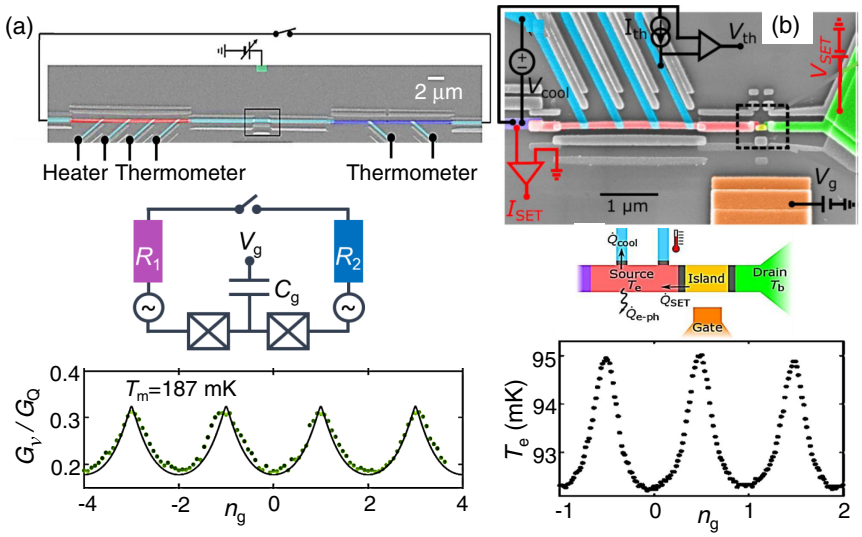

FIG. 14. (a) SEM (top panel) and the equivalent electrical circuit diagram (middle panel) of the device including a Cooper-pair transistor coupled to two normal-metal resistors R_1 and R_2 at temperatures T_1 and T_2, respectively. Bottom panel: measured thermal conductance (symbols) normalized by G_Q as a function of gate charge $n_g = C_g V_g / e$ at $T_m = (T_1 + T_2)/2$. The solid line indicates the theoretical expectation. Adapted from Maillet *et al.*, 2020. (b) SEM image (top panel) and schematic realization (middle panel) of the device consisting of a single-electron transistor and the heat transport measurement setup. The black circuit in the top left corner displays the heat transport setup. Bottom panel: measured gate dependence of the electronic temperature T_e of the source island when it is lower than the bath temperature T_0. Adapted from Dutta *et al.*, 2017.

electrical conductance go hand in hand. Yet deviations from the Wiedemann-Franz law due to a Coulomb blockade and quantum tunneling were observed, in agreement with theory (Kubala, König, and Pekola, 2008; Rodionov, Burmistrov, and Chtchelkatchev, 2010).

A. Electronic quantum heat interferometer

Another quantum interference experiment on heat current by electrons was performed by Giazotto and Martínez-Pérez (2012) (shown in Fig. 15). They used a magnetic-field-controlled SQUID as an interferometer. They could independently measure the electrical and heat transport via the device. For the latter, the SQUID was placed between two mesoscopic heat baths and the heat current was measured with the principle depicted in Fig. 2(b). The measurement was performed in a temperature regime exceeding that described in Sec. IV.A such that T is high enough for the superconductor to have a substantial equilibrium quasiparticle population (i.e., not all electrons are paired). In this regime the superconductor as such can support heat current, and heat interference across the Josephson junctions of the SQUID becomes possible. Giazotto and Martínez-Pérez (2012) addressed experimentally for the first time a half-century-old proposal and theory (Maki and Griffin, 1965); more recent work was given by Guttman *et al.* (1997), Guttman, Ben-Jacob, and Bergman (1998), Zhao, Löfwander, and Sauls (2003), and Golubev, Faivre, and Pekola (2013). Giazotto and Martínez-Pérez (2012) also demonstrated the potential of electronic caloritronics in superconducting circuits.

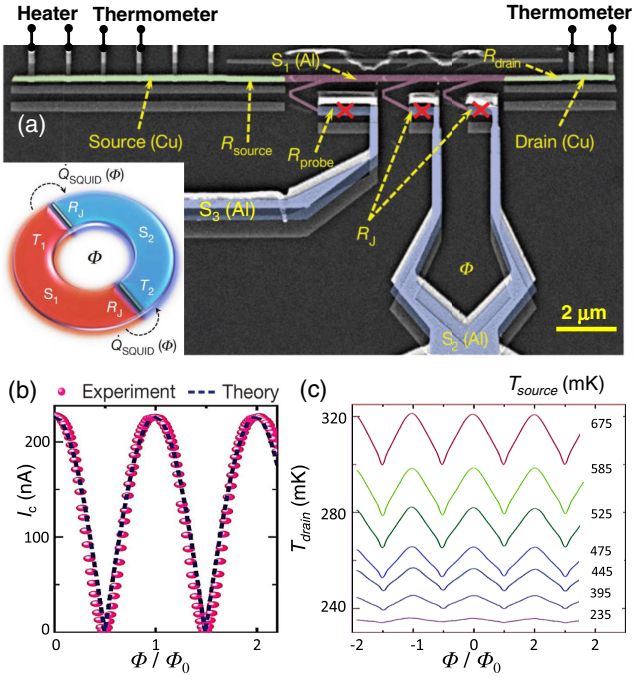

FIG. 15. Josephson heat interferometer. (a) SEM of the device. The source and drain electrodes made out of Cu are connected to an Al island (S_1) through two AlO_x tunnel barriers. S_1 is connected sideways to a dc SQUID that terminates at a large-volume lead S_2 (Al) for thermalization and to an Al tunnel probe (S_3) for independent SQUID characterization. *N-I-S* junctions in source and drain are used to heat and monitor the temperature of each island. Red crosses indicate the Josephson junctions. The core of the device (SQUID) is shown schematically in the inset. Two identical superconductors with different temperatures are connected with the two tunnel junctions of the SQUID. When the magnetic flux Φ is applied, the heat current $\dot{Q}_{SQUID}(\Phi)$ from hot to cold varies. (b) Maximal charge current of the SQUID I_c as a function of Φ at 240 mK bath temperature. The dashed line presents the theoretical result assuming 0.3% asymmetry in the junctions, and symbols represent experimental data. (c) Flux modulation of T_{drain} related to heat current measured at different T_{source} values. Here the bath temperature is fixed at 235 mK. Adapted from Giazotto and Martínez-Pérez, 2012.

B. Cooling a quantum circuit

In the experiment performed by Tan *et al.* (2017) photon-assisted tunneling serves the purpose of decreasing the number of microwave quanta in a superconducting quantum circuit, namely, a coplanar wave resonator (harmonic oscillator). The optical micrograph of the sample presented in Fig. 16(a) shows resistive elements inserted at the two ends of the resonator, acting as heat sinks for it. Figure 16(b) displays the temperature of one of these resistors [a quantum circuit refrigerator (QCR)], measured and controlled by *N-I-S* tunneling, effectively lowering and elevating the electronic temperature of it depending on the biasing of the cooler junction; see Sec. IV.B. The other resistor ("probe") is passive but its temperature is likewise monitored. This temperature reacts weakly to the QCR temperature changes. Tan *et al.* (2017) developed a thermal model based on which they extracted the average number of photons in the resonator

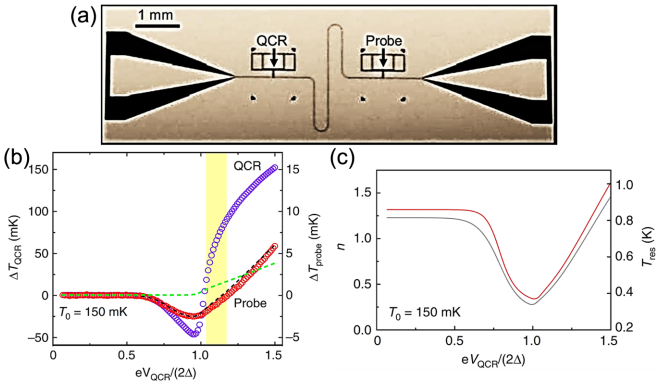

FIG. 16. Quantum circuit refrigerator (QCR). (a) Optical micrograph of a sample where a superconducting coplanar-waveguide resonator is in the center coupled to a QCR and a probe resistor indicated by the arrows. (b) Measured changes in the electron temperature of the QCR ΔT_{QCR} (purple circles) and the probe resistor ΔT_{probe} (red circles) as functions of the refrigerator operation voltage V_{QCR}. The black dashed line, closely following the probe data, and green dashed line show the given theoretical results on ΔT_{probe}, including and excluding photon-assisted tunneling, respectively. (c) Average number of photons n and the corresponding effective temperature of the resonator T_{res}, shown as the solid lines in red and gray, based on the thermal model introduced by Tan *et al.* (2017). Adapted from Tan *et al.*, 2017.

and the corresponding temperature $T_{\rm res}$. In this experiment $T_{\rm res} \approx 800$ mK far exceeds all other temperatures, most notably the electronic temperatures of the two resistors $T_{\rm QCR} \approx T_{\rm probe} \approx 150$ mK, even under no bias on the QCR. The model then predicts cooling of the resonator down to about 400 mK under optimal biasing conditions of the QCR [Fig. 16(c)]. Based on the parameters given by Tan *et al.* (2017), one would estimate the resonator to have $T_{\rm res} \approx$ 200 mK when the QCR is not biased. Indeed, in a later work (Masuda *et al.*, 2018) resonator temperatures in the 200 mK regime were reported at zero bias. When biased, the *N*-*I*-*S* junctions operate as an incoherent microwave source. The mode temperature of the resonator can then be driven even beyond 2.5 K, far above the temperature of the phonon and electron reservoirs of the system (Masuda *et al.*, 2018). This phenomenon was theoretically modeled by Silveri *et al.* (2017) using photon-assisted tunneling of the biased *N*-*I*-*S* junctions as the environment. The effective temperature of the resonator is expected to be lifted to $\sim eV/(2k_B)$ at bias voltage V.

IX. QUANTUM HEAT TRANSPORT MEDIATED BY A SUPERCONDUCTING QUBIT

In this section we introduce a superconducting qubit as an element that mediates heat by microwave photons between two baths. Different types of superconducting quantum bits, such as flux, charge, and transmon qubits, are options in such devices (Clarke and Wilhelm, 2008). They feature different coupling options and strengths, as well as different degrees of anharmonicity in the Josephson potential, which is discussed later. In the experiments of Ronzani *et al.* (2018) transmon-type qubits, introduced by Koch *et al.* (2007), were employed. This kind of qubit has levels whose positions can be controlled by magnetic flux through the SQUID loop. A transmon qubit is only weakly anharmonic, meaning that one typically needs to consider not only the two lowest levels that form the actual qubit but also the higher levels in this nearly harmonic potential. We point out an important difference: although even weak anharmonicity is enough to address only the two lowest levels in a microwave-driven experiment, one needs, on the contrary, to consider higher levels as well when the qubit sees a thermal bath with a wide spectrum. Yet in a typical experiment described later, the separation of the levels is of the order of 0.5 K, meaning that the thermal population of the third level is already small at the low temperatures of the experiment, say, below 0.2 K ($\sim e^{-5} < 0.01$).

In this section we present thermal transport experiments under conditions in which the qubit is not driven. Coherent properties of the qubit do not then play an important role. In the future the same devices will be driven by rf fields, and the off-diagonal elements of the density matrix will evolve as well.

A. Quantum heat valve

Figure 17(a) (top panel) shows a typical experimental configuration of heat control with a qubit from Ronzani *et al.* (2018). The energy separation of the transmon qubit [Fig. 17(a), center] can be controlled by the external magnetic flux Φ. The qubit is coupled capacitively (coupling g) to two nominally identical superconducting coplanar wave resonators that act as LC resonators with resonant frequencies of ~5 GHz each. For thermal transport experiments the $\lambda/4$ resonators are terminated by on-chip resistors that form the controlled dissipative elements in the circuit (Chang *et al.*, 2019). The dissipation is then given by the inverse of the quality factor of the resonator and can be quantified by another coupling parameter γ. In this circuit, which is called a quantum heat valve, heat is carried wirelessly (via capacitors) by thermal microwave photons over a distance of a few millimeters from one bath to another. A schematic model of such a coupled circuit is shown at the top of Figs. 17(b) and 17(c).

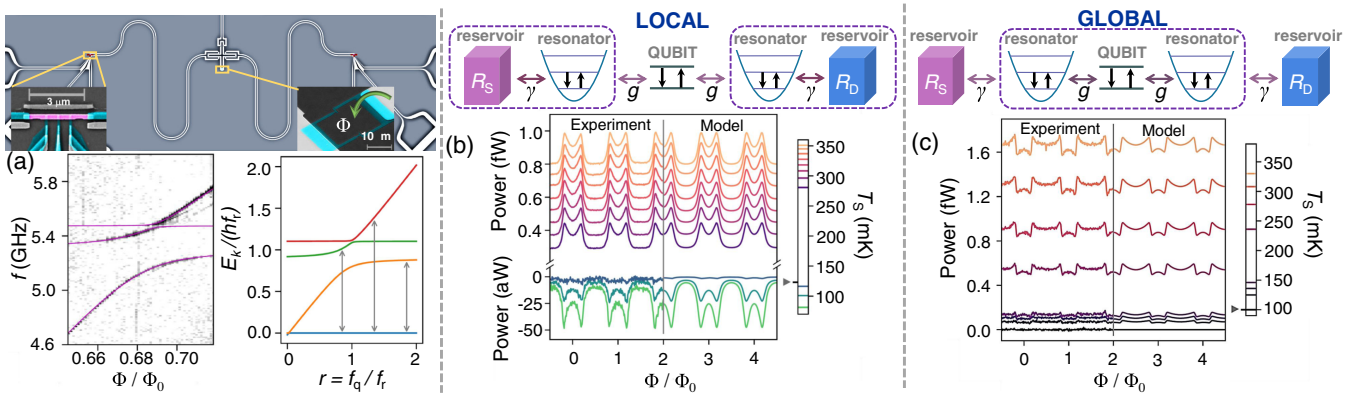

FIG. 17. Quantum heat valve: the local and global regimes. (a) Quantum heat valve device (top panel) where the transmon-type superconducting qubit in the center is capacitively coupled to two similar $\lambda/4$ coplanar-waveguide resonators made out of Nb. Each resonator terminates with a normal-metal resistor (Cu) acting as a reservoir. Insets: SEM images of the SQUID that can be controlled by magnetic flux Φ, and one of the two reservoirs (pink, in the center) whose temperature is monitored and controlled by *N*-*I*-*S* probes (Cu-AlO_x-Al). The lower panels show the two-tone transmission spectroscopy (left panel) and the corresponding theoretical positions (right panel) for the structure shown on top without resistors. (b),(c) Schematic illustrations of the two regimes (top panels). The resulting heat transport data are shown in the lower panels, where the flux dependence of the heat current in the drain reservoir in the two regimes is measured. Each trace corresponds to a different temperature T_S of the source reservoir shown in the legend bar. Adapted from Ronzani *et al.*, 2018.

It turns out that the measurement of heat transport in such a circuit addresses some fundamental questions of open quantum systems (Rivas *et al.*, 2010; Levy and Kosloff, 2014; Purkayastha, Dhar, and Kulkarni, 2016a; Hofer *et al.*, 2017; De Chiara *et al.*, 2018; Donvil *et al.*, 2018; Aurell and Montana, 2019; Magazzù and Grifoni, 2019; Donvil, Muratore-Ginanneschi, and Golubev, 2020; Hewgill, De Chiara, and Imparato, 2020). There are at least two possible ways of viewing the circuit, namely, the local view [Fig. 17(b)] and the global view [Fig. 17(c)]. In the local picture as we define it, the environment of the qubit is formed from the dissipative LC resonator with Lorentzian noise spectrum centered around its resonance frequency. In this regime, which occurs when $\gamma \gg g$, the system indeed acts as a valve admitting heat current to pass through only when the qubit frequency matches (within the range determined by the quality factor) the frequency of the resonators. This results in Lorentzian peaks in power centered at flux positions corresponding to said matching condition, demonstrated by both experiment and theory, shown in the bottom panel of Fig. 17(b). In the opposite limit, in the global regime when $\gamma \ll g$, the situation is different. The combined system composed of the resonators and the qubit then makes up a hybrid that interacts with the bare environment formed of the two resistors. In this limit the hybrid quantum system has the energy spectrum shown in the bottom panel of Fig. 17(a) exhibiting a multilevel structure. This is shown by the basic calculated spectrum and the spectroscopic measurement on a structure similar to that in the top panel but in the absence of the resistive loads. The data in Fig. 17(c) demonstrate results in the global regime, with the experiment and theory developed by Ronzani *et al.* (2018) in agreement with each other. This experiment is the first one to assess local-global crossover in the spirit of locating the Heisenberg cut between the quantum and classical worlds. In a recent theoretical analysis, we analyzed the crossover behavior between the two limiting regimes with the help of a direct solution of the Schrödinger equation including an oscillator bath (Pekola and Karimi, 2020).

B. Thermal rectifier

In a symmetric structure, as in Fig. 17, there is naturally no directional dependence of heat transport between the two baths. However, heat current rectification becomes possible if one breaks the symmetry of the structure (Segal and Nitzan, 2005). Heat recitification (Ruokola, Ojanen, and Jauho, 2009; Sothmann *et al.*, 2012; Sánchez, Sothmann, and Jordan, 2015; Purkayastha, Dhar, and Kulkarni, 2016b; Motz *et al.*, 2018; Goury and Sánchez, 2019; Kargı *et al.*, 2019; Riera-Campeny *et al.*, 2019; Bhandari *et al.*, 2021; Iorio *et al.*, 2021) can be quantified in different ways, but in general finite rectification means that the magnitudes of forward and reverse heat currents differ under identical but opposite temperature biasing conditions. There have been a few experiments on heat current rectification, including ones on phonons in carbon nanotubes (Chang *et al.*, 2006), electrons in quantum dots (Scheibner *et al.*, 2008), mesoscopic tunnel junctions (Martínez-Pérez, Fornieri, and Giazotto, 2015), and suspended graphene (Wang *et al.*, 2017). Senior *et al.* (2020) realized rectification in a structure similar to that in Fig. 17 but by making the two resonators unequal in length: the two resonators had in this case frequencies of 3 and 7 GHz. An additional feature necessary for heat rectification is the nonlinearity of the central element, which arises from the anharmonicity of the transmon Josephson potential. Figure 18 shows data from Senior *et al.* (2020) where heat current through the structure is measured in forward and reverse directions under the same but opposite temperature biasing, respectively. Complicated flux dependence can be observed, but the main feature is that one reaches 10% rectification at best and that it depends strongly on the flux position determining the coupling asymmetry to the two baths. A quantitative analysis of the flux dependence is challenging and experiments in simpler setups would be welcome.

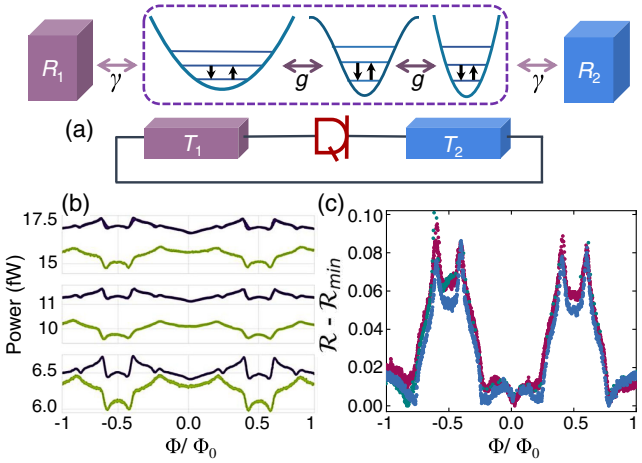

FIG. 18. Heat rectification using a transmon qubit. (a) Schematic illustration of a photon diode composed of an anharmonic oscillator (qubit) coupled to two LC resonators with largely different resonance frequencies. Bottom panel: circuit view of the system where we assign the quantum heat rectifier in the middle with a red symbol. (b) Dependence of source-drain heat current (power) as a function of magnetic flux in forward ($1 \to 2$, dark line, P^+) and reverse ($2 \to 1$, light-colored line, P^-) directions under identical but opposite bias conditions at a few different source temperatures (420, 400, and 380 mK from top to bottom). (c) Rectification ratio $\mathcal{R} = P^+/P^-$ (with its minimal value subtracted) as a function of magnetic flux for the data in (b) at the three temperatures of the source. Adapted from Senior *et al.*, 2020.

X. HEAT CURRENT NOISE

In this section we focus on fluctuations of currents, which are generally considered to be harmful and something to get rid of. The synonym of fluctuations, noise, proposes this negative side of the concept of fluctuations. Noise typically determines the minimal detectable signal in a measurement, i.e., the resolution. Here we do not consider noise caused by the measurement apparatus or from other extrinsic sources, but we instead focus on intrinsic noise due to fundamental quantum and thermal fluctuations. This noise, for instance, in the form of electrical current or heat current fluctuations, determines the ultimate achievable measurement accuracy. But besides being a limiting factor of a measurement, noise can serve as a signal to build on in order to realize a sensor: for instance, measurement of thermal current noise of a conductor

provides one of the most popular and fundamental thermometers in use (Fleischmann, Reiser, and Enss, 2020).

We already discussed current and voltage noise of a linear dissipative element in Sec. IV.D. Here we review the heat current noise, both classical and quantum; see Sánchez and Büttiker (2012), Moskalets (2014), Pekola and Karimi (2018), Miller *et al.* (2020), Crépieux (2021), Eriksson *et al.* (2021), and Karimi and Pekola (2021). For simplicity, we first consider the tunneling as an example. Besides presenting the classical fluctuation-dissipation theorem for heat current, which we review in a general case after the presentation, we observe the quantum expression of heat current noise, including the frequency-dependent component due to zero point fluctuations surviving down to $T = 0$. Next we focus on the temperature dynamics of a finite system coupled to a bath, which yields the experimentally accessible fundamental fluctuations of the effective temperature of this subsystem. Finally, we review the experimental situation, which currently consists of only a small number of examples, on fluctuations in heat transport of quantum and classical systems.

A. FDT for heat in tunneling

We consider tunneling where the average heat current out from lead L was given by Eq. (18). Taking for simplicity the normal conductors (*N-I-N* junction) with $n_{\mathrm{L}}(\epsilon) = n_{\mathrm{R}}(\epsilon) = 1$, we have the following average heat current at $eV = 0$:

$$\dot{Q}_{\mathrm{L}} = \frac{1}{e^2 R_T}\int d\epsilon\, \epsilon[f_{\mathrm{L}}(\epsilon) - f_{\mathrm{R}}(\epsilon)]. \tag{39}$$

The thermal conductance for tunneling $G_{\mathrm{th}} = d\dot{Q}_{\mathrm{L}}/dT_{\mathrm{L}}|_{T_{\mathrm{L}}=T}$ is then given by $G_{\mathrm{th}} = \mathcal{L}TG_T$, where $G_T = 1/R_T$ is the conductance of the tunnel junction. Like the fully transmitting channels in Sec. II, the tunnel junction satisfies the Wiedemann-Franz law.

The heat current operator $\dot{\hat{H}}_{\mathrm{L}}$ to obtain the average heat current of Eq. (18) was calculated using the tunnel coupling operator of Eq. (16) and commuting it with the Hamiltonian of the left lead. We may use this operator to find the two-time correlator of it and Fourier transform it to find the spectral density of noise of the heat current at finite angular frequency ω (but at $eV = 0$) as $S_{\dot{Q}}(\omega) = \int dt\langle\dot{\hat{H}}_{\mathrm{L}}(t)\dot{\hat{H}}_{\mathrm{L}}(0)\rangle e^{i\omega t}$, yielding (Averin and Pekola, 2010; Sergi, 2011; Zhan, Denisov, and Hänggi, 2013; Karimi and Pekola, 2021)

$$S_{\dot{Q}}(\omega) = \frac{G_T}{6e^2}[(2\pi k_B T)^2 + (\hbar\omega)^2]\frac{\hbar\omega}{1 - e^{-\hbar\omega/k_B T}}. \tag{40}$$

For the symmetrized noise $S^{(\mathrm{s})}_{\dot{Q}}(\omega) = (1/2)[S_{\dot{Q}}(\omega) + S_{\dot{Q}}(-\omega)]$, we then have

$$S^{(\mathrm{s})}_{\dot{Q}}(\omega) = \frac{G_T}{12e^2}[(2\pi k_B T)^2 + (\hbar\omega)^2]\hbar\omega\,\coth\left(\frac{\hbar\omega}{2k_B T}\right). \tag{41}$$

Now there are two important limits to consider. First, for $\omega \to 0$ we obtain the classical fluctuation-dissipation theorem for heat current as

$$S^{(\mathrm{s})}_{\dot{Q}}(0) = 2k_B T^2 G_{\mathrm{th}}. \tag{42}$$

Second, on the other hand, the finite frequency noise does not vanish at zero temperature, but

$$S^{(\mathrm{s})}_{\dot{Q}}(\omega) = \frac{G_T}{12e^2}|\hbar\omega|^3, \qquad T = 0. \tag{43}$$

B. FDT for heat for a general system

Section X.A serves as an illustration of how noise and dissipation are related. Here we extend the discussion to a general setup beyond the tunneling case. This allows us to treat other mechanisms as well, for instance, the phonons, photons, and electron-phonon coupling relevant to this Colloquium. In general the FDT for heat applies in the form introduced in Eq. (42) for low frequency noise. To see this we may write the Hamiltonian

$$\hat{\mathcal{H}} = \hat{H}_{\mathrm{s}} + \hat{H}_{\mathrm{b}} + \hat{H}_{\mathrm{c}} \equiv \hat{H}_0 + \hat{H}_{\mathrm{c}}, \tag{44}$$

where the unperturbed Hamiltonian $\hat{H}_0 = \hat{H}_{\mathrm{s}} + \hat{H}_{\mathrm{b}}$ is composed of the system and bath and $\hat{H}_{\mathrm{c}}$ is again the coupling. In linear response, we then have the expectation value of the heat current to the system

$$\dot{Q} = \langle\dot{\hat{H}}_{\mathrm{s}}\rangle = -\frac{i}{\hbar}\int_{-\infty}^{0} dt'\langle[\dot{\hat{H}}_{\mathrm{s}}(0), \hat{H}_{\mathrm{c}}(t')]\rangle_0. \tag{45}$$

The expectation value of a general operator $\mathcal{O}$ in the noninteracting system is written as $\langle\mathcal{O}\rangle_0 = \mathrm{Tr}(e^{-\beta_{\mathrm{s}}\hat{H}_{\mathrm{s}}}e^{-\beta\hat{H}_{\mathrm{b}}}\mathcal{O})/\mathrm{Tr}(e^{-\beta_{\mathrm{s}}\hat{H}_{\mathrm{s}}}e^{-\beta\hat{H}_{\mathrm{b}}})$, where $\beta_{\mathrm{s}} = (k_B T_{\mathrm{s}})^{-1}$ and $\beta = (k_B T)^{-1}$ are the corresponding inverse temperatures of the system and bath, respectively. By definition, the thermal conductance is given by

$$G_{\mathrm{th}} = -\left.\frac{d\dot{Q}}{dT_{\mathrm{s}}}\right|_{T_{\mathrm{s}}=T} = \frac{1}{k_B T^2}\langle\delta\hat{H}_{\mathrm{s}}\dot{\hat{H}}_{\mathrm{s}}\rangle_0, \tag{46}$$

where we used $\hat{H}_{\mathrm{s}} - \langle\hat{H}_{\mathrm{s}}\rangle_0 \equiv \delta\hat{H}_{\mathrm{s}}$. On the other hand, the spectral density of noise for the heat current at zero frequency is given by

$$S_{\dot{Q}}(0) = \int_{-\infty}^{\infty} dt'\langle\dot{\hat{H}}_{\mathrm{s}}(t')\dot{\hat{H}}_{\mathrm{s}}(0)\rangle_0, \tag{47}$$

which is analogous to what was introduced in the tunneling case. After some algebra and a careful comparison of Eqs. (46) and (47), we find the FDT given in Eq. (42).

C. Effective temperature fluctuations

Here we consider a system with varying temperature $T(t)$. This setup, shown in Fig. 2(a), presents an absorber of a calorimeter or bolometer coupled via thermal conductance G_{th} to a heat bath at fixed temperature T_0. If we further assume that the small system has the heat capacity $\mathcal{C}$, the energy balance equation reads for the heat current $\dot{Q}(t)$ between the bath and the absorber

$$\dot{Q}(t) = \mathcal{C}\delta\dot{T}(t) + G_{\rm th}\delta T(t), \tag{48}$$

where $\delta T(t)$ is the difference between the absorber temperature and that of the bath. To calculate thermal noise, we again evaluate the two-time correlator as

$$\langle \dot{Q}(t)\dot{Q}(0)\rangle = \mathcal{C}^2\langle \delta\dot{T}(t)\delta\dot{T}(0)\rangle + G_{\rm th}^2\langle \delta T(t)\delta T(0)\rangle, \tag{49}$$

which leads to

$$S_{\dot{Q}}(\omega) = (\omega^2\mathcal{C}^2 + G_{\rm th}^2)S_T(\omega). \tag{50}$$

Since we typically consider frequencies well below the temperature, $S_{\dot{Q}}(\omega)$ is essentially frequency independent [which was shown in Eq. (41) for tunneling], and the classical FDT holds for $S_{\dot{Q}}(0)$ in the form of Eq. (42) in equilibrium. Thus, we have

$$S_T(\omega) = \frac{2k_BT_0^2}{G_{\rm th}}\frac{1}{1+(\omega\tau)^2}, \tag{51}$$

where $\tau = \mathcal{C}/G_{\rm th}$ is the thermal relaxation time. This means that in the low frequency limit $S_T(0) = 2k_BT^2/G_{\rm th}$. The root-mean-square (rms) fluctuation of temperature is obtained as the inverse Fourier transform of the noise spectrum at $t = 0$ as

$$\langle \delta T^2\rangle = \int_{-\infty}^{\infty}\frac{d\omega}{2\pi}S_T(\omega) = \frac{k_BT_0^2}{\mathcal{C}}, \tag{52}$$

which is the well-known textbook result for temperature fluctuations (Lifshitz and Pitaevskii, 1980; Heikkilä and Nazarov, 2009; van den Berg, Brange, and Samuelsson, 2015). The results of Eqs. (51) and (52) are directly accessible in experiments.

D. Progress on measuring fluctuations of heat current and entropy

The previous discussion applies for systems and processes in or near equilibrium. In recent decades relations that also hold far from equilibrium and for finite times have been developed (Bochkov and Kuzovlev, 1981; Jarzynski, 1997; Crooks, 1999; Seifert, 2012). During the past 20 years they have also become experimentally feasible thanks mainly to advances in the production and manipulation of nanostructures. The best known nonequilibrium fluctuation relations governing entropy production ΔS are given by $P(\Delta S)/P(-\Delta S) = e^{\Delta S/k_B}$ and its corollary $\langle e^{-\Delta S/k_B}\rangle = 1$. Here $\langle\cdot\rangle$ refers to the average over many experimental realizations or to the expectation value for the measurement. For macroscopic systems near equilibrium these relations simplify to the second law of thermodynamics.

Here we give a summary of such nonequilibrium experiments on electrical systems. Fluctuations of entropy production and heat currents have been actively studied experimentally for more than a decade in the classical regime, but mainly via indirect means of detection since entropy is a tricky quantity for a direct measurement (Kleeorin *et al.*, 2019). Two main classes of systems under study have been those in seminal experiments on molecules (Collin *et al.*, 2005) and electrical circuits (Küng *et al.*, 2012; Saira, Yoon *et al.*, 2012; Ciliberto *et al.*, 2013; Pekola, 2015; Bérut *et al.*, 2016; Cottet *et al.*, 2017). Other works go beyond FDT by addressing far-from-equilibrium fluctuation relations (Bochkov and Kuzovlev, 1981; Jarzynski, 1997; Crooks, 1999; Campisi, Hänggi, and Talkner, 2011; Seifert, 2012; Pekola and Khaymovich, 2019). As shown in Fig. 19(a), Ciliberto *et al.* (2013) examined the setup of two macroscopic resistors at temperatures near the ambient. An indirect measurement of entropy was facilitated by Ciliberto *et al.* (2013) via the detection of instantaneous electrical power IV, integrated over time and divided by the corresponding temperature of the macroscopic resistor. This way several fluctuation relations for entropy production under nonequilibrium conditions (Seifert, 2005, 2012) could be verified together with the standard FDT in the linear response regime. Similarly, in the setup of Saira, Yoon *et al.* (2012) shown in Fig. 19(b),

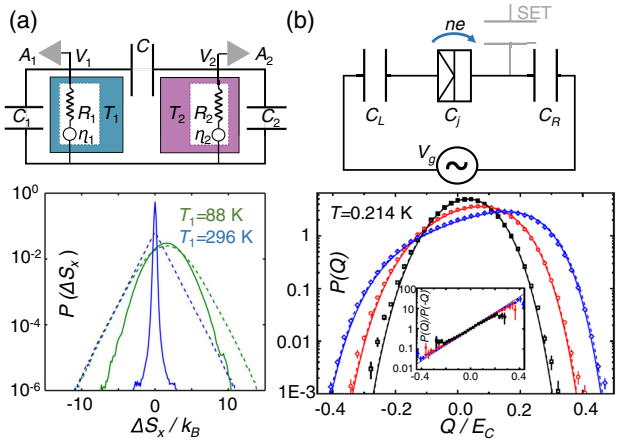

FIG. 19. Indirect measurements of noise of heat current and entropy production. (a) Circuit diagram (upper panel) where two resistors R_1 and R_2 at temperatures T_1 and $T_2 = 296$ K, respectively, are coupled via the capacitance C. C_i, V_i, and A_i, with $i = 1, 2$, schematically show the capacitance of the cables and input amplifiers, applied voltages, and low noise amplifiers, respectively. The probability of the entropy production due to the heat exchanged with the reservoirs $P(\Delta S_r)$ (dashed lines) and the probability of the total entropy $P(\Delta S_{\rm tot})$ (solid lines) measured at different temperatures. Blue lines correspond to equilibrium, where both distributions are centered symmetrically around zero, and green lines represent an out-of-equilibrium case with distributions shifted toward a positive value. Adapted from Ciliberto *et al.*, 2013. (b) Electron box (upper panel) formed by two metallic electrodes that are coupled using a tunnel junction with capacitance C_j and connected capacitively to the voltage source via $C_{\rm L}$ and $C_{\rm R}$. The box is also connected to a single-electron transistor (SET) working as an electrometer indicated with a gray line. Lower panel: measured distribution of the generated heat $P(Q)$ at three different drive frequencies: 1 (black squares), 2 (red circles), and 4 Hz (blue diamonds). The solid lines are exact theoretical predictions, and the dashed lines show the results of Monte Carlo simulations. Inset: solid line displays the Crooks fluctuation theorem, and the symbols indicate the $P(Q)/P(-Q)$ ratio for the experimental distributions. Adapted from Saira, Yoon *et al.*, 2012.

detecting single electrons making nonequilibrium transitions across a junction in a single-electron box provides indirect means of observing the dissipated energy and entropy production quantitatively (Averin and Pekola, 2011; Koski *et al.*, 2013). These experiments were performed at temperatures 3 orders of magnitude lower than in the work of Ciliberto *et al.* (2013). The relations of Crooks (1999) and Jarzynski (1997) as well as generalized relations incorporating the role of information in the Maxwell's demon setup (Sagawa and Ueda, 2010) could be tested accurately in these experiments (Pekola and Khaymovich, 2019).

The reason for using indirect measurement of heat by detailed electrical characterization is the fact that the powers are far too small to resolve with direct thermometry (Sec. III.B). Next we focus on progress related to the direct measurement of heat current fluctuations.

E. Energy sensitivity of a calorimeter

The ultimate energy resolution of a thermal detector (see Fig. 20) is determined by the coupling of it to the heat bath associated with the fluctuations of the heat current. Taking a wideband thermometer on a calorimeter, the rms fluctuations of the effective temperature due to this intrinsic noise are given by Eq. (52). To find the energy resolution of the detector one needs to compare this noise to the impact of the absorption of energy E on the temperature of the detector, which can be evaluated by solving Eq. (48) for an instantaneous absorption of a photon at energy E at the time instant $t = 0$, meaning that $\dot{Q}(t) = E\delta(t)$ with the solution $\delta T(t) = (E/\mathcal{C})e^{-t/\tau}\theta(t)$, where the time constant $\tau = \mathcal{C}/G_{\rm th}$ and $\theta(t)$ is the Heaviside step function. Thus, at $t = 0+$ the immediate rise of T is $\delta T(0) = E/\mathcal{C}$. The signal-to-noise ratio $\mathbb{SNR} = \delta T(0)/\sqrt{\langle \delta T^2 \rangle}$ is

$$\mathbb{SNR} = E/\sqrt{k_B T_0^2 \mathcal{C}}, \tag{53}$$

meaning that the energy resolution of the detector in this regime is

$$\delta E = \sqrt{k_B T_0^2 \mathcal{C}}. \tag{54}$$

For convenience, we write $\mathcal{C} = \eta k_B$, where η is a dimensionless constant that we assess later. We then find that $\delta E = \sqrt{\eta} k_B T_0$. As an example, related to the experiment of Karimi *et al.* (2020) we take a metallic calorimeter where $\mathcal{C} = \gamma \mathcal{V} T_0$ at low temperatures; see Figs. 20(a) and 20(b). Here $\gamma \sim 100\ \mathrm{J\,K^{-2}\,m^{-3}}$ for copper and $\mathcal{V} < 10^{-21}\ \mathrm{m^3}$ is the volume of the absorber, yielding $\eta \sim 100$ and the energy resolution $\delta E/k_B \sim 0.1\ \mathrm{K}$ at $T_0 = 0.01\ \mathrm{K}$ (Karimi and Pekola, 2020).

Fluctuations in power have a direct impact on the performance of the calorimeters and bolometers (Irwin, 1995; Gildemeister, Lee, and Richards, 2001), i.e., thermal detectors of radiation. This noise determines the energy resolution of a calorimeter, and also the noise-equivalent power under continuous irradiation, as in the measurement of the cosmic microwave background (Mather, 1982). Direct measurements

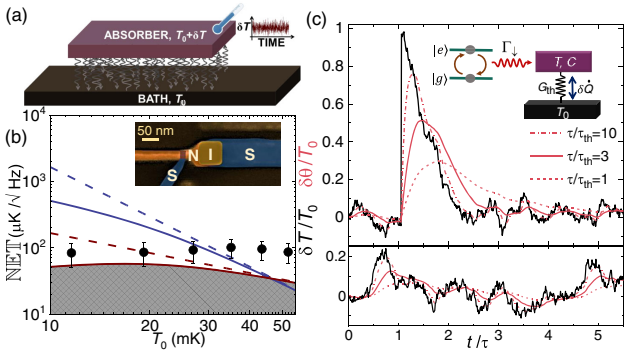

FIG. 20. Quantum calorimeter. (a) Normal-metal absorber coupled to the phonon heat bath at the fixed temperature T_0 via electron-phonon collisions, indicated by many arrows. These collisions lead to a stochastic exchange of heat between the absorber and the bath, and to the fluctuating temperature δT in the absorber. The core of the device is the calorimeter including a thermometer, which measures the temporal temperature variations. An example of a temperature trace is shown next to the absorber. Adapted from Karimi *et al.*, 2020. (b) Noise-equivalent temperature of the calorimeter. The solid symbols are the measured signal of temperature fluctuations at equilibrium $[\mathbb{NET} \equiv \sqrt{S_T} = \sqrt{\langle \delta T^2 \rangle/(2\Delta f)}]$ obtained via the measurement of $\langle \delta T^2 \rangle$ with $\Delta f = 10$ kHz. The solid and dashed lines represent the noise-equivalent temperature in equilibrium $\mathbb{NET}$ of the normal-metal absorber in the presence and absence of an extra photon contribution, respectively. Red lines (the two lower lines) display $\mathbb{NET}$ at equilibrium ($\mathbb{NET}_{\rm eq} = \sqrt{2k_B T_0^2/G_{\rm th}}$), while the blue lines (the two upper lines) show $\mathbb{NET} = \delta\epsilon/\sqrt{\mathcal{C}G_{\rm th}}$, which is the required $\mathbb{NET}$ of a detector to observe a photon with energy $\delta\epsilon = 1\ \mathrm{K} \times k_B$. The prohibited range bordered by the fundamental temperature fluctuations at equilibrium is indicated by the shaded area. Inset: scanning electron micrograph of part of the actual sensor, the *S*-*N*-*I*-*S* structure, where Cu is used as a normal-metal *N* and Al as a superconductor *S*. The *S*-*N*-*I*-*S* junction is the dissipative element in the *RLC* circuit operating at $f_0 \approx 650$ MHz. Adapted from Karimi and Pekola, 2020. (c) Simulation of the expected thermometer signal of a calorimeter in response to the absorption of an incoming photon depicted in the inset. The parameters of the simulation of the detector correspond to the experiment shown in (b), with $\eta \equiv \mathcal{C}/k_B = 100$ and $\hbar\omega_{\rm Q}/(k_B T_0) = 100$, where $\hbar\omega_{\rm Q}$ is the qubit energy and $T_0 = 10$ mK. The noise seen in the traces is the result of temperature fluctuations due to the coupling of the absorber to the phonon bath. Upper panel: jump occurring at $t/\tau = 1$ (the time instant set arbitrarily), which exceeds the noise level of equilibrium fluctuations, with a signal-to-noise ratio of about 10. The red lines (truncated by filtering) show the results at different cutoff frequencies of the thermometer parametrized by the ratio of the electron-phonon time and the detector response time.

of fluctuating temperature are rare (Chui *et al.*, 1992; Karimi *et al.*, 2020). The pioneering measurement of Chui *et al.* (1992) employed a macroscopic calorimeter working at the so-called lambda point of liquid helium, i.e., its superfluid transition temperature at $T = 2.17$ K. Chui *et al.* (1992) managed to verify Eqs. (51) and (52) thanks to a high resolution of the thermometer measuring the magnetization of a paramagnetic salt (copper ammonium bromide) with the

help of a SQUID down to a 10^{-10} K/$\sqrt{\text{Hz}}$ noise-equivalent temperature.

The nanofabricated detector of Karimi *et al.* (2020) worked in the regime where the measurement cutoff frequency was 10 kHz, which falls somewhat below $1/\tau$. Furthermore, the metallic absorber was proximitized by a superconducting contact further decreasing $\mathcal{C}$ and G_{th} (Heikkilä and Giazotto, 2009; Nikolic, Basko, and Belzig, 2020) and thus improving its performance. The experiment [Fig. 20(b)], which utilized a superconductor–normal-metal–insulator–superconductor (*S*-*N*-*I*-*S*) thermometer (Karimi and Pekola, 2018), demonstrated noise of the effective temperature of the calorimeter that is close to the expected fundamental fluctuation limit of Eq. (51) at low frequencies, at the same time promising a $\mathbb{SNR}$ of ∼10 in measuring an absorption event with the photon energy $E/k_B = 1$ K. Figure 20(c) demonstrates by simulation the validity of the previous analysis. The wideband detector would present T fluctuations that are an order of magnitude smaller than the temperature jump due to the 1 K photon absorption event. In summary, this measurement demonstrates the feasibility of a microwave photon measurement using a metallic calorimeter at $T_0 = 10$ mK.

There exist several other concepts of ultrasensitive thermal detectors, either metallic ones (Govenius *et al.*, 2016; Kuzmin *et al.*, 2019) or those utilizing graphene or semiconductors (Roukes, 1999; Kokkoniemi *et al.*, 2019; Lara-Avila *et al.*, 2019; Kokkoniemi *et al.*, 2020; Lee *et al.*, 2020), or those based on temperature-dependent magnetization (Christian, 2005; Kempf *et al.*, 2018). The advantage of graphene is its supposedly low heat capacity, which could make the thermal response time shorter than in metal detectors. Yet none of the proposed detectors has demonstrated detection of quanta in said microwave regime to date.

XI. SUMMARY AND OUTLOOK

In this Colloquium we focused on the fundamental aspects of quantum heat transport, with the main emphasis on experiments carried out during the past 20 years. In many respects the physics of heat transport in quantum nanostructures is currently well understood, and experiments tend to confirm the theoretical predictions. In some systems clean experiments are, however, more difficult to realize than in others from a practical point of view, and more experiments are needed: one example is presented by one-dimensional phonon structures, where pioneering experiments were performed long ago (Schwab *et al.*, 2000), but where precise conditions regarding how to realize ballistic contacts are still under debate. Experiments on quantum heat transport serve also as tools to understand quantum matter itself, as recent experiments in the fractional quantum Hall regime demonstrate (Banerjee *et al.*, 2017; Dutta *et al.*, 2021). On the other hand, they provide us with ways of realizing new kinds of devices and determining how to nail down and achieve their ultimate limits of performance. We discussed the latter issue in Sec. X on noise in heat current.

As to the potentially useful devices based on quantum heat transport, we now discuss two examples. The first one is a rather straightforward application of heat management on chip for quantum information processes. Microwave photons provide a means to transport quanta and energy in general over large distances, as we discussed in Sec. VII.C. It could thus serve as a way to reset quantum circuits rapidly. There is, however, a trade-off to be considered. Rapid thermalization is almost a synonym for a low quality factor and fast decoherence in a quantum system, which are not desirable properties. Therefore, tunable coupling is a possible way to go, to switch on and off the coupling to a heat bath on demand. Variations of the many heat valves presented in this Colloquium could in principle serve the purpose. Tests of such an idea were proposed and experimented on by Partanen *et al.* (2018).

Quantum heat engines and cyclic refrigerators are presently under intensive study; see Humphrey and Linke (2005), Quan *et al.* (2007), Deffner, Jarzynski, and Campo (2014), Pilgram, Sánchez, and López (2015), Campisi and Fazio (2016), Benenti *et al.* (2017), Brandner, Bauer, and Seifert (2017), Alicki and Kosloff (2018), Josefsson *et al.* (2018), Bhandari *et al.* (2020), Majidi *et al.* (2021), and Raja *et al.* (2021). Experiments that are fully in the quantum regime have thus far been practically nonexistent, although there have been proposals addressing realistic setups (Abah *et al.*, 2012; Karimi and Pekola, 2016). For instance, a so-called quantum Otto cycle can be realized by alternately coupling a superconducting qubit to two different heat baths (Karimi and Pekola, 2016). If this is done by varying the energy level separation of the qubit, as was done in the photonic heat valve or rectifier earlier, but now cyclically at rf frequencies, one can extract heat from the cold bath and dump it into the hot one when system parameters are chosen properly. We expect devices of this type or analogous ones to work in the near future. Interesting questions arise as to whether one can boost the powers and/or efficiencies by exploiting quantum dynamics, and as to which kinds of protocols can speed up the cycles for higher powers in general (Funo *et al.*, 2019; Menczel *et al.*, 2019; Solfanelli, Falsetti, and Campisi, 2020).

We note here that topological matter (Hasan and Kane, 2010; Qi and Zhang, 2011), specifically topological superconductors and Josephson junctions, have been proposed as potential novel elements in quantum thermodynamics and heat transport experiments due to their unconventional physical properties, see the recent work of Rivas and Martin-Delgado (2017), Bauer and Sothmann (2019), Scharf *et al.* (2020), and Pan, Sau, and Das Sarma (2021). Owing to the focus of the current paper, mainly on experiments, we do not discuss this topic further.

In this Colloquium we alluded to the connections of heat transport and quantum thermodynamics, mainly regarding concrete device concepts, including thermal detectors, heat engines, and refrigerators. On a more fundamental level, quantum heat transport is at the heart of open quantum systems physics (Breuer and Petruccione, 2002), with the non-Hermitian dynamics governed by the quantum noise (Gardiner and Zoller, 2010) widely discussed in this Colloquium. True thermodynamics counts on observations of heat currents and temperatures, and power consumption of the sources. Adopting this view, one can pose many questions, such as how to measure work and heat in an open quantum system, for which the measurement apparatus cannot be viewed as an innocent witness of what is happening in the quantum system itself. The calorimeter can eventually become

the microscope of quantum dynamics on the level of the exchange of energy by individual quanta emitted or absorbed by the quantum system. This would give us the optimal tool to investigate stochastic thermodynamics in the true quantum regime. Many other fundamentally and practically important questions will arise and can potentially be answered by heat transport experiments. For instance, how does a quantum system thermalize, and does it find an equilibrium thermal state even in the absence of a heat bath? To conclude, investigations and exploitation of quantum heat transport will play an important role in the currently active field of quantum thermodynamics and in future quantum technologies in general.

ACKNOWLEDGMENTS

This work was supported by Academy of Finland Grant No. 312057, the European Union's Horizon 2020 research and innovation program under the Marie Skłodowska-Curie actions (Grant Agreement No. 766025), the Russian Science Foundation (Grant No. 20-62-46026), and the Foundational Questions Institute Fund (FQXi) via Grant No. FQXi-IAF19-06.

REFERENCES

Abah, O., J. Roßnagel, G. Jacob, S. Deffner, F. Schmidt-Kaler, K. Singer, and E. Lutz, 2012, "Single-Ion Heat Engine at Maximum Power," Phys. Rev. Lett. **109**, 203006.

Alicki, Robert, and Ronnie Kosloff, 2018, in *Thermodynamics in the Quantum Regime: Fundamental Aspects and New Directions*, edited by Felix Binder, Luis A. Correa, Christian Gogolin, Janet Anders, and Gerardo Adesso (Springer, New York).

Altimiras, C., H. le Sueur, U. Gennser, A. Cavanna, D. Mailly, and F. Pierre, 2010, "Tuning Energy Relaxation along Quantum Hall Channels," Phys. Rev. Lett. **105**, 226804.

Ashcroft, Neil W., and N. David Mermin, 1976, *Solid State Physics* (Holt, Rinehart and Winston, New York).

Aurell, Erik, and Federica Montana, 2019, "Thermal power of heat flow through a qubit," Phys. Rev. E **99**, 042130.

Averin, D. V., and K. K. Likharev, 1991, in *Mesoscopic Phenomena in Solids*, Modern Problems in Condensed Matter Sciences, edited by B. L. Altshuler, P. A. Lee, and R. A. Webb (Elsevier Science, Amsterdam).

Averin, D. V., and J. P. Pekola, 2011, "Statistics of the dissipated energy in driven single-electron transitions," Europhys. Lett. **96**, 67004.

Averin, Dmitri V., and Jukka P. Pekola, 2010, "Violation of the Fluctuation-Dissipation Theorem in Time-Dependent Mesoscopic Heat Transport," Phys. Rev. Lett. **104**, 220601.

Banerjee, Mitali, Moty Heiblum, Amir Rosenblatt, Yuval Oreg, Dima E. Feldman, Ady Stern, and Vladimir Umansky, 2017, "Observed quantization of anyonic heat flow," Nature (London) **545**, 75–79.

Banerjee, Mitali, Moty Heiblum, Vladimir Umansky, Dima E. Feldman, Yuval Oreg, and Ady Stern, 2018, "Observation of half-integer thermal Hall conductance," Nature (London) **559**, 205.

Bardeen, J., L. N. Cooper, and J. R. Schrieffer, 1957, "Theory of superconductivity," Phys. Rev. **108**, 1175–1204.

Bardeen, J., G. Rickayzen, and L. Tewordt, 1959, "Theory of the thermal conductivity of superconductors," Phys. Rev. **113**, 982–994.

Bauer, Alexander G., and Björn Sothmann, 2019, "Phase-dependent heat transport in Josephson junctions with *p*-wave superconductors and superfluids," Phys. Rev. B **99**, 214508.

Benenti, Giuliano, Giulio Casati, Keiji Saito, and Robert S. Whitney, 2017, "Fundamental aspects of steady-state conversion of heat to work at the nanoscale," Phys. Rep. **694**, 1–124.

Bérut, A., A. Imparato, A. Petrosyan, and S. Ciliberto, **2016**, "The role of coupling on the statistical properties of the energy fluxes between stochastic systems at different temperatures," J. Stat. Mech. 054002.

Bhandari, Bibek, Paolo Andrea Erdman, Rosario Fazio, Elisabetta Paladino, and Fabio Taddei, 2021, "Thermal rectification through a nonlinear quantum resonator," Phys. Rev. B **103**, 155434.

Bhandari, Bibek, Pablo Terrén Alonso, Fabio Taddei, Felix von Oppen, Rosario Fazio, and Liliana Arrachea, 2020, "Geometric properties of adiabatic quantum thermal machines," Phys. Rev. B **102**, 155407.

Blencowe, Miles P, and Vincenzo Vitelli, 2000, "Universal quantum limits on single-channel information, entropy, and heat flow," Phys. Rev. A **62**, 052104.

Bochkov, G. N., and Yu. E. Kuzovlev, 1981, "Nonlinear fluctuation-dissipation relations and stochastic models in nonequilibrium thermodynamics: I. Generalized fluctuation-dissipation theorem," Physica (Amsterdam) **106A**, 443–479.

Brandner, Kay, Michael Bauer, and Udo Seifert, 2017, "Universal Coherence-Induced Power Losses of Quantum Heat Engines in Linear Response," Phys. Rev. Lett. **119**, 170602.

Breuer, H.-P., and F. Petruccione, 2002, *The Theory of Open Quantum Systems* (Oxford University Press, New York).

Bruus, Henrik, and Karsten Flensberg, 2004, *Many-Body Quantum Theory in Condensed Matter Physics* (Oxford University Press, New York).

Butcher, P. N., 1990, "Thermal and electrical transport formalism for electronic microstructures with many terminals," J. Phys. Condens. Matter **2**, 4869–4878.

Callen, Herbert B., and Theodore A. Welton, 1951, "Irreversibility and generalized noise," Phys. Rev. **83**, 34–40.

Campisi, Michele, and Rosario Fazio, 2016, "The power of a critical heat engine," Nat. Commun. **7**, 11895.

Campisi, Michele, Peter Hänggi, and Peter Talkner, 2011, "Colloquium: Quantum fluctuation relations: Foundations and applications," Rev. Mod. Phys. **83**, 771–791.

Chang, C. W., D. Okawa, A. Majumdar, and A. Zettl, 2006, "Solid-state thermal rectifier," Science **314**, 1121–1124.

Chang, Yu-Cheng, Bayan Karimi, Jorden Senior, Alberto Ronzani, Joonas T. Peltonen, Hsi-Sheng Goan, Chii-Dong Chen, and Jukka P. Pekola, 2019, "Utilization of the superconducting transition for characterizing low-quality-factor superconducting resonators," Appl. Phys. Lett. **115**, 022601.

Chiatti, O., J. T. Nicholls, Y. Y. Proskuryakov, N. Lumpkin, I. Farrer, and D. A. Ritchie, 2006, "Quantum Thermal Conductance of Electrons in a One-Dimensional Wire," Phys. Rev. Lett. **97**, 056601.

Christian, Enss, 2005, Ed., *Cryogenic Particle Detection* (Springer, Berlin).

Chui, T. C. P., D. R. Swanson, M. J. Adriaans, J. A. Nissen, and J. A. Lipa, 1992, "Temperature Fluctuations in the Canonical Ensemble," Phys. Rev. Lett. **69**, 3005–3008.

Ciliberto, S., A. Imparato, A. Naert, and M. Tanase, 2013, "Heat Flux and Entropy Produced by Thermal Fluctuations," Phys. Rev. Lett. **110**, 180601.

Clark, A. M., A. Williams, S. T. Ruggiero, M. L. van den Berg, and J. N. Ullom, 2004, "Practical electron-tunneling refrigerator," Appl. Phys. Lett. **84**, 625–627.

Clarke, John, and Frank K. Wilhelm, 2008, "Superconducting quantum bits," Nature (London) **453**, 1031–1042.

Collin, D., F. Ritort, C. Jarzynski, S. B. Smith, I. Tinoco, Jr., and C. Bustamante, 2005, "Verification of the Crooks fluctuation theorem and recovery of RNA folding free energies," Nature (London) **437**, 231–234.

Cottet, N., S. Jezouin, L. Bretheau, P. Campagne-Ibarcq, Q. Ficheux, J. Anders, A. Auffèves, R. Azouit, P. Rouchon, and B. Huard, 2017, "Observing a quantum Maxwell demon at work," Proc. Natl. Acad. Sci. U.S.A. **114**, 7561–7564.

Courtois, H., F. W. J. Hekking, H. Q. Nguyen, and C. B. Winkelmann, 2014, "Electronic coolers based on superconducting tunnel junctions: Fundamentals and applications, J. Low Temp. Phys. **175**, 799–812.

Crépieux, A., 2021, "Electronic heat current fluctuations in a quantum dot," Phys. Rev. B **103**, 045427.

Crooks, Gavin E., 1999, "Entropy production fluctuation theorem and the nonequilibrium work relation for free energy differences," Phys. Rev. E **60**, 2721–2726.

Cui, Longji, Wonho Jeong, Sunghoon Hur, Manuel Matt, Jan C. Klöckner, Fabian Pauly, Peter Nielaba, Juan Carlos Cuevas, Edgar Meyhofer, and Pramod Reddy, 2017, "Quantized thermal transport in single-atom junctions," Science **355**, 1192–1195.

De Chiara, Gabriele, Gabriel Landi, Adam Hewgill, Brendan Reid, Alessandro Ferraro, Augusto J. Roncaglia, and Mauro Antezza, 2018, "Reconciliation of quantum local master equations with thermodynamics," New J. Phys. **20**, 113024.

Deffner, Sebastian, Christopher Jarzynski, and Adolfo del Campo, 2014, "Classical and Quantum Shortcuts to Adiabaticity for Scale-Invariant Driving," Phys. Rev. X **4**, 021013.

Donvil, Brecht, Paolo Muratore-Ginanneschi, and Dmitry Golubev, 2020, "Exactly solvable model of calorimetric measurements," Phys. Rev. B **102**, 245401.

Donvil, Brecht, Paolo Muratore-Ginanneschi, Jukka P. Pekola, and Kay Schwieger, 2018, "Model for calorimetric measurements in an open quantum system," Phys. Rev. A **97**, 052107.

Dutta, B., J. T. Peltonen, D. S. Antonenko, M. Meschke, M. A. Skvortsov, B. Kubala, J. König, C. B. Winkelmann, H. Courtois, and J. P. Pekola, 2017, "Thermal Conductance of a Single-Electron Transistor," Phys. Rev. Lett. **119**, 077701.

Dutta, Bivas, Wenmin Yang, Ron Aharon Melcer, Hemanta Kumar Kundu, Moty Heiblum, Vladimir Umansky, Yuval Oreg, Ady Stern, and David Mross, 2021, "Novel method distinguishing between competing topological orders," arXiv:2101.01419.

Eriksson, J., M. Acciai, L. Tesser, and J. Splettstoesser, 2021, "General Bounds on Electronic Shot Noise in the Absence of Currents," Phys. Rev. Lett. **127**, 136801.

Feshchenko, A. V., J. V. Koski, and J. P. Pekola, 2014, "Experimental realization of a Coulomb blockade refrigerator," Phys. Rev. B **90**, 201407.

Feshchenko, A. V., O.-P. Saira, J. T. Peltonen, and J. P. Pekola, 2017, "Thermal conductance of Nb thin films at sub-kelvin temperatures," Sci. Rep. **7**, 41728.

Fleischmann, A., A. Reiser, and C. Enss, 2020, "Noise thermometry for ultralow temperatures, J. Low Temp. Phys. **201**, 803–824.

Funo, Ken, Neill Lambert, Bayan Karimi, Jukka P. Pekola, Yuta Masuyama, and Franco Nori, 2019, "Speeding up a quantum refrigerator via counterdiabatic driving," Phys. Rev. B **100**, 035407.

Gantmakher, V. F., 1974, "The experimental study of electron-phonon scattering in metals," Rep. Prog. Phys. **37**, 317.

Gardiner, C. W., and P. Zoller, 2010, *Quantum Noise* (Springer-Verlag, Berlin).

Giazotto, Francesco, Tero T. Heikkilä, Arttu Luukanen, Alexander M. Savin, and Jukka P. Pekola, 2006, "Opportunities for mesoscopics in thermometry and refrigeration: Physics and applications," Rev. Mod. Phys. **78**, 217–274.

Giazotto, Francesco, and María José Martínez-Pérez, 2012, "The Josephson heat interferometer," Nature (London) **492**, 401–405.

Gildemeister, Jan M., Adrian T. Lee, and Paul L. Richards, 2001, "Model for excess noise in voltage-biased superconducting bolometers," Appl. Opt. **40**, 6229–6235.

Golubev, D. S., and J. P. Pekola, 2015, "Statistics of heat exchange between two resistors," Phys. Rev. B **92**, 085412.

Golubev, Dmitry, Timothé Faivre, and Jukka P. Pekola, 2013, "Heat transport through a Josephson junction," Phys. Rev. B **87**, 094522.

Goury, Donald, and Rafael Sánchez, 2019, "Reversible thermal diode and energy harvester with a superconducting quantum interference single-electron transistor," Appl. Phys. Lett. **115**, 092601.

Govenius, J., R. E. Lake, K. Y. Tan, and M. Möttönen, 2016, "Detection of Zeptojoule Microwave Pulses Using Electrothermal Feedback in Proximity-Induced Josephson Junctions," Phys. Rev. Lett. **117**, 030802.

Granger, G., J. P. Eisenstein, and J. L. Reno, 2009, "Observation of Chiral Heat Transport in the Quantum Hall Regime," Phys. Rev. Lett. **102**, 086803.

Guttman, Glen D., Eshel Ben-Jacob, and David J. Bergman, 1998, "Interference effect heat conductance in a Josephson junction and its detection in an rf SQUID," Phys. Rev. B **57**, 2717–2719.

Guttman, Glen D., Benny Nathanson, Eshel Ben-Jacob, and David J. Bergman, 1997, "Phase-dependent thermal transport in Josephson junctions," Phys. Rev. B **55**, 3849–3855.

Halbertal, D., *et al.*, 2016, "Nanoscale thermal imaging of dissipation in quantum systems," Nature (London) **539**, 407.

Halbertal, Dorri, *et al.*, 2017, "Imaging resonant dissipation from individual atomic defects in graphene," Science **358**, 1303.

Hasan, M. Z., and C. L. Kane, 2010, "Colloquium: Topological insulators," Rev. Mod. Phys. **82**, 3045–3067.

Heikkilä, T. T., and Francesco Giazotto, 2009, "Phase sensitive electron-phonon coupling in a superconducting proximity structure," Phys. Rev. B **79**, 094514.

Heikkilä, T. T., and Yuli V. Nazarov, 2009, "Statistics of Temperature Fluctuations in an Electron System out of Equilibrium," Phys. Rev. Lett. **102**, 130605.

Hewgill, Adam, Gabriele De Chiara, and Alberto Imparato, 2020, "Quantum thermodynamically consistent local master equations," arXiv:2008.04742.

Hofer, Patrick P., Martí Perarnau-Llobet, L. David M Miranda, Géraldine Haack, Ralph Silva, Jonatan Bohr Brask, and Nicolas Brunner, 2017, "Markovian master equations for quantum thermal machines: Local versus global approach," New J. Phys. **19**, 123037.

Humphrey, T. E., and H. Linke, 2005, "Quantum, cyclic, and particle-exchange heat engines," Physica (Amsterdam) **29E**, 390–398.

Iorio, A., E. Strambini, G. Haack, M. Campisi, and F. Giazotto, 2021, "Photonic Heat Rectification in a System of Coupled Qubits," Phys. Rev. Applied **15**, 054050.

Irwin, K. D., 1995, "An application of electrothermal feedback for high resolution cryogenic particle detection," Appl. Phys. Lett. **66**, 1998.

Jarzynski, C., 1997, "Nonequilibrium Equality for Free Energy Differences," Phys. Rev. Lett. **78**, 2690–2693.

Jezouin, S., F. D. Parmentier, A. Anthore, U. Gennser, A. Cavanna, Y. Jin, and F. Pierre, 2013, "Quantum limit of heat flow across a single electronic channel," Science **342**, 601–604.

Johnson, J. B., 1928, "Thermal agitation of electricity in conductors," Phys. Rev. **32**, 97–109.

Josefsson, Martin, Artis Svilans, Adam M. Burke, Eric A. Hoffmann, Sofia Fahlvik, Claes Thelander, Martin Leijnse, and Heiner Linke, 2018, "A quantum-dot heat engine operating close to the thermodynamic efficiency limits," Nat. Nanotechnol. **13**, 920.

Josephson, B. D., 1962, "Possible new effects in superconductive tunnelling," Phys. Lett. **1**, 251–253.

Kane, C. L., and Matthew P. A. Fisher, 1997, "Quantized thermal transport in the fractional quantum Hall effect," Phys. Rev. B **55**, 15832–15837.

Kargı, Cahit, M. Tahir Naseem, Tomáš Opatrný, Özgür E. Müstecaplıoğlu, and Gershon Kurizki, 2019, "Quantum optical two-atom thermal diode," Phys. Rev. E **99**, 042121.

Karimi, B., and J. P. Pekola, 2016, "Otto refrigerator based on a superconducting qubit: Classical and quantum performance," Phys. Rev. B **94**, 184503.

Karimi, Bayan, Fredrik Brange, Peter Samuelsson, and Jukka P. Pekola, 2020, "Reaching the ultimate energy resolution of a quantum detector," Nat. Commun. **11**, 367.

Karimi, Bayan, and Jukka P. Pekola, 2018, "Noninvasive Thermometer Based on the Zero-Bias Anomaly of a Superconducting Junction for Ultrasensitive Calorimetry," Phys. Rev. Applied **10**, 054048.

Karimi, Bayan, and Jukka P. Pekola, 2020, "Quantum Trajectory Analysis of Single Microwave Photon Detection by Nanocalorimetry," Phys. Rev. Lett. **124**, 170601.

Karimi, Bayan, and Jukka P. Pekola, 2021, "Down-conversion of quantum fluctuations of photonic heat current in a circuit," arXiv:2104.09238.

Kempf, S., A. Fleischmann, L. Gastaldo, and C. Enss, 2018, "Physics and applications of metallic magnetic calorimeters, J. Low Temp. Phys. **193**, 365–379.

Kjaergaard, Morten, Mollie E. Schwartz, Jochen Braumüller, Philip Krantz, Joel I.-J. Wang, Simon Gustavsson, and William D. Oliver, 2020, "Superconducting qubits: Current state of play," Annu. Rev. Condens. Matter Phys. **11**, 369–395.

Kleeorin, Yaakov, Holger Thierschmann, Hartmut Buhmann, Antoine Georges, Laurens W. Molenkamp, and Yigal Meir, 2019, "How to measure the entropy of a mesoscopic system via thermoelectric transport," Nat. Commun. **10**, 5801.

Koch, Jens, Terri M. Yu, Jay Gambetta, A. A. Houck, D. I. Schuster, J. Majer, Alexandre Blais, M. H. Devoret, S. M. Girvin, and R. J. Schoelkopf, 2007, "Charge-insensitive qubit design derived from the Cooper pair box," Phys. Rev. A **76**, 042319.

Kokkoniemi, R., *et al.*, 2020, "Bolometer operating at the threshold for circuit quantum electrodynamics," Nature (London) **586**, 47–51.

Kokkoniemi, Roope, *et al.*, 2019, "Nanobolometer with ultralow noise equivalent power," Commun. Phys. **2**, 124.

Koski, J. V., T. Sagawa, O-P. Saira, Y. Yoon, A. Kutvonen, P. Solinas, M. Möttönen, T. Ala-Nissila, and J. P. Pekola, 2013, "Distribution of entropy production in a single-electron box," Nat. Phys. **9**, 644–648.

Krantz, P., M. Kjaergaard, F. Yan, T. P. Orlando, S. Gustavsson, and W. D. Oliver, 2019, "A quantum engineer's guide to superconducting qubits," Appl. Phys. Rev. **6**, 021318.

Kubala, Björn, Jürgen König, and Jukka Pekola, 2008, "Violation of the Wiedemann-Franz Law in a Single-Electron Transistor," Phys. Rev. Lett. **100**, 066801.

Kubo, Ryogo, 1957, "Statistical-mechanical theory of irreversible processes. I. General theory and simple applications to magnetic and conduction problems, J. Phys. Soc. Jpn. **12**, 570–586.

Küng, B., C. Rössler, M. Beck, M. Marthaler, D. S. Golubev, Y. Utsumi, T. Ihn, and K. Ensslin, 2012, "Irreversibility on the Level of Single-Electron Tunneling," Phys. Rev. X **2**, 011001.

Kuzmin, L., I. Agulo, M. Fominsky, A. Savin, and M. Tarasov, 2004, "Optimization of electron cooling by SIN tunnel junctions," Supercond. Sci. Technol. **17**, S400–S405.

Kuzmin, L. S., A. L. Pankratov, A. V. Gordeeva, V. O. Zbrozhek, V. A. Shamporov, L. S. Revin, A. V. Blagodatkin, S. Masi, and P. de Bernardis, 2019, "Photon-noise-limited cold-electron bolometer based on strong electron self-cooling for high-performance cosmology missions," Commun. Phys. **2**, 104.

Landauer, Rolf, 1981, "Can a length of perfect conductor have a resistance?," Phys. Lett. **85A**, 91.

Lara-Avila, S., A. Danilov, D. Golubev, H. He, K. H. Kim, R. Yakimova, F. Lombardi, T. Bauch, S. Cherednichenko, and S. Kubatkin, 2019, "Towards quantum-limited coherent detection of terahertz waves in charge-neutral graphene," Nat. Astron. **3**, 983–988.

Lee, Gil-Ho, *et al.*, 2020, "Graphene-based Josephson junction microwave bolometer," Nature (London) **586**, 42–46.

Leivo, M. M., and J. P. Pekola, 1998, "Thermal characteristics of silicon nitride membranes at sub-kelvin temperatures," Appl. Phys. Lett. **72**, 1305.

Leivo, M. M., J. P. Pekola, and D. V. Averin, 1996, "Efficient Peltier refrigeration by a pair of normal metal/insulator/superconductor junctions," Appl. Phys. Lett. **68**, 1996.

Leivo, Mikko, 1999, "On-chip cooling by quasiparticle tunneling below 1 kelvin," Ph.D. thesis (University of Jyväskylä).

le Sueur, H., C. Altimiras, U. Gennser, A. Cavanna, D. Mailly, and F. Pierre, 2010, "Energy Relaxation in the Integer Quantum Hall Regime," Phys. Rev. Lett. **105**, 056803.

Levy, Amikam, and Ronnie Kosloff, 2014, "The local approach to quantum transport may violate the second law of thermodynamics," Europhys. Lett. **107**, 20004.

Lifshitz, E. M., and L. P. Pitaevskii, 1980, *Statistical Physics: Part I*, 3rd ed., Course of Theoretical Physics Vol. 5 (Pergamon Press, New York).

Lounasmaa, O. V., 1974, *Experimental Principles and Methods Below 1K* (Academic Press, New York).

Magazzù, L., and M. Grifoni, **2019**, "Transmission spectra of an ultrastrongly coupled qubit-dissipative resonator system," J. Stat. Mech. 104002.

Maillet, Olivier, Diego Subero, Joonas T. Peltonen, Dmitry S. Golubev, and Jukka P. Pekola, 2020, "Electric field control of radiative heat transfer in a superconducting circuit," Nat. Commun. **11**, 4326.

Majidi, D., M. Josefsson, M. Kumar, M. Leijnse, L. Samuelson, H. Courtois, C. B. Winkelmann, and V. F. Maisi, 2021, "Quantum confinement suppressing electronic heat flow below the Wiedemann-Franz law," arXiv:2106.06229.

Maki, Kazumi, and Allan Griffin, 1965, "Entropy Transport between Two Superconductors by Electron Tunneling," Phys. Rev. Lett. **15**, 921–923.

Manninen, A. J., M. M. Leivo, and J. P. Pekola, 1997, "Refrigeration of a dielectric membrane by superconductor/insulator/normal-metal/insulator/superconductor tunneling, Appl. Phys. Lett. **70**, 1885.

Martínez-Pérez, Maria José, Antonio Fornieri, and Francesco Giazotto, 2015, "Rectification of electronic heat current by a hybridthermal diode," Nat. Nanotechnol. **10**, 303–307.

Masuda, Shumpei, Kuan Y. Tan, Matti Partanen, Russell E. Lake, Joonas Govenius, Matti Silveri, Hermann Grabert, and Mikko Möttönen, 2018, "Observation of microwave absorption and emission from incoherent electron tunneling through a normal-metal–insulator–superconductor junction," Sci. Rep. **8**, 3966.

Mather, John C, 1982, "Bolometer noise: Nonequilibrium theory," Appl. Opt. **21**, 1125–1129.

Menczel, Paul, Tuomas Pyhäranta, Christian Flindt, and Kay Brandner, 2019, "Two-stroke optimization scheme for mesoscopic refrigerators," Phys. Rev. B **99**, 224306.

Meschke, Matthias, Wiebke Guichard, and Jukka P. Pekola, 2006, "Single-mode heat conduction by photons," Nature (London) **444**, 187–190.

Miller, Harry J. D., Giacomo Guarnieri, Mark T. Mitchison, and John Goold, 2020, "Quantum Fluctuations Hinder Finite-Time Information Erasure near the Landauer Limit," Phys. Rev. Lett. **125**, 160602.

Molenkamp, L. W., Th. Gravier, H. van Houten, O. J. A. Buijk, M. A. A. Mabesoone, and C. T. Foxon, 1992, "Peltier Coefficient and Thermal Conductance of a Quantum Point Contact," Phys. Rev. Lett. **68**, 3765–3768.

Moskalets, Michael, 2014, "Floquet Scattering Matrix Theory of Heat Fluctuations in Dynamical Quantum Conductors," Phys. Rev. Lett. **112**, 206801.

Mosso, Nico, Ute Drechsler, Fabian Menges, Peter Nirmalraj, Siegfried Karg, Heike Riel, and Bernd Gotsmann, 2017, "Heat transport through atomic contacts," Nat. Nanotechnol. **12**, 430–433.

Motz, T., M. Wiedmann, J. T. Stockburger, and J. Ankerhold, 2018, "Rectification of heat currents across nonlinear quantum chains: A versatile approach beyond weak thermal contact," New J. Phys. **20**, 113020.

Muhonen, Juha T., Matthias Meschke, and Jukka P. Pekola, 2012, "Micrometre-scale refrigerators," Rep. Prog. Phys. **75**, 046501.

Nahum, M., T. M. Eiles, and John M. Martinis, 1994, "Electronic microrefrigerator based on a normal-insulator-superconductor tunnel junction," Appl. Phys. Lett. **65**, 3123.

Nakamura, Y., Yu. A. Pashkin, and J. S. Tsai, 1999, "Coherent control of macroscopic quantum states in a single-Cooper-pair box," Nature (London) **398**, 786–788.

Nam, Seung-Geol, E. H. Hwang, and Hu-Jong Lee, 2013, "Thermoelectric Detection of Chiral Heat Transport in Graphene in the Quantum Hall Regime," Phys. Rev. Lett. **110**, 226801.

Nguyen, H. Q., T. Aref, V. J. Kauppila, M. Meschke, C. B. Winkelmann, H. Courtois, and J. P. Pekola, 2013, "Trapping hot quasi-particles in a high-power superconducting electronic cooler," New J. Phys. **15**, 085013.

Nikolic, Danilo, Denis M. Basko, and Wolfgang Belzig, 2020, "Electron cooling by phonons in superconducting proximity structures," Phys. Rev. B **102**, 214514.

Nyquist, H., 1928, "Thermal agitation of electric charge in conductors," Phys. Rev. **32**, 110–113.

Pan, Haining, Jay D. Sau, and S. Das Sarma, 2021, "Three-terminal nonlocal conductance in Majorana nanowires: Distinguishing topological and trivial in realistic systems with disorder and inhomogeneous potential," Phys. Rev. B **103**, 014513.

Partanen, M., K. Y. Tan, J. Govenius, R. E. Lake, M. K. Mäkelä, T. Tanttu, and M. Möttönen, 2016, "Quantum-limited heat conduction over macroscopic distances," Nat. Phys. **12**, 460.

Partanen, M., *et al.*, 2018, "Flux-tunable heat sink for quantum electric circuits," Sci. Rep. **8**, 6325.

Pascal, L. M. A., H. Courtois, and F. W. J. Hekking, 2011, "Circuit approach to photonic heat transport," Phys. Rev. B **83**, 125113.

Pekola, J. P., and I. M. Khaymovich, 2019, "Thermodynamics in single-electron circuits and superconducting qubits," Annu. Rev. Condens. Matter Phys. **10**, 193–212.

Pekola, Jukka P., 2015, "Towards quantum thermodynamics in electronic circuits," Nat. Phys. **11**, 118–123.

Pekola, Jukka P., and Bayan Karimi, 2018, "Quantum noise of electron-phonon heat current, J. Low Temp. Phys. **191**, 373–379.

Pekola, Jukka P., and Bayan Karimi, 2020, "Qubit decay in circuit quantum thermodynamics," arXiv:2010.11122.

Peltonen, J. T., P. Virtanen, M. Meschke, J. V. Koski, T. T. Heikkilä, and J. P. Pekola, 2010, "Thermal Conductance by the Inverse Proximity Effect in a Superconductor," Phys. Rev. Lett. **105**, 097004.

Pendry, J., 1983, "Quantum limits to the flow of information and entropy," J. Phys. A **16**, 2161–2171.

Pilgram, S., D. Sánchez, and R. López, 2015, "Quantum point contacts as heat engines," Physica (Amsterdam) **74E**, 447–450.

Pothier, H., S. Guéron, Norman O. Birge, D. Esteve, and M. H. Devoret, 1997, "Energy Distribution Function of Quasiparticles in Mesoscopic Wires," Phys. Rev. Lett. **79**, 3490–3493.

Prance, J. R., C. G. Smith, J. P. Griffiths, S. J. Chorley, D. Anderson, G. A. C. Jones, I. Farrer, and D. A. Ritchie, 2009, "Electronic Refrigeration of a Two-Dimensional Electron Gas," Phys. Rev. Lett. **102**, 146602.

Purkayastha, Archak, Abhishek Dhar, and Manas Kulkarni, 2016a, "Out-of-equilibrium open quantum systems: A comparison of approximate quantum master equation approaches with exact results," Phys. Rev. A **93**, 062114.

Purkayastha, Archak, Abhishek Dhar, and Manas Kulkarni, 2016b, "Nonlinear transport in an out-of-equilibrium single-site Bose-Hubbard model: Scaling, rectification, and time dynamics," Phys. Rev. A **94**, 052134.

Qi, Xiao-Liang, and Shou-Cheng Zhang, 2011, "Topological insulators and superconductors," Rev. Mod. Phys. **83**, 1057–1110.

Quan, H. T., Yu-xi Liu, C. P. Sun, and Franco Nori, 2007, "Quantum thermodynamic cycles and quantum heat engines," Phys. Rev. E **76**, 031105.

Raja, S. Hamedani, S. Maniscalco, G. S. Paraoanu, J. P. Pekola, and N. L. Gullo, 2021, "Finite-time quantum stirling heat engine," New J. Phys. **23**, 033034.

Rego, Luis G. C., and George Kirczenow, 1998, "Quantized Thermal Conductance of Dielectric Quantum Wires," Phys. Rev. Lett. **81**, 232–235.

Rego, Luis G. C., and George Kirczenow, 1999, "Fractional exclusion statistics and the universal quantum of thermal conductance: A unifying approach," Phys. Rev. B **59**, 13080–13086.

Riera-Campeny, Andreu, Mohammad Mehboudi, Marisa Pons, and Anna Sanpera, 2019, "Dynamically induced heat rectification in quantum systems," Phys. Rev. E **99**, 032126.

Rivas, Ángel, A. Douglas, K. Plato, Susana F. Huelga, and Martin B. Plenio, 2010, "Markovian master equations: A critical study," New J. Phys. **12**, 113032.

Rivas, Ángel, and Miguel A. Martin-Delgado, 2017, "Topological heat transport and symmetry-protected boson currents," Sci. Rep. **7**, 6350.

Rodionov, Ya. I., I. S. Burmistrov, and N. M. Chtchelkatchev, 2010, "Relaxation dynamics of the electron distribution in the Coulomb-blockade problem," Phys. Rev. B **82**, 155317.

Ronzani, Alberto, Bayan Karimi, Jorden Senior, Yu-Cheng Chang, Joonas T. Peltonen, ChiiDong Chen, and Jukka P. Pekola, 2018, "Tunable photonic heat transport in a quantum heat valve," Nat. Phys. **14**, 991.

Roukes, M. L., 1999, "Yoctocalorimetry: Phonon counting in nanostructures," Physica (Amsterdam) **263B–264B**, 1–15.

Roukes, M. L., M. R. Freeman, R. S. Germain, R. C. Richardson, and M. B. Ketchen, 1985, "Hot Electrons and Energy Transport in Metals at Millikelvin Temperatures," Phys. Rev. Lett. **55**, 422–425.

Ruokola, Tomi, Teemu Ojanen, and Antti-Pekka Jauho, 2009, "Thermal rectification in nonlinear quantum circuits," Phys. Rev. B **79**, 144306.

Sagawa, Takahiro, and Masahito Ueda, 2010, "Generalized Jarzynski Equality under Nonequilibrium Feedback Control," Phys. Rev. Lett. **104**, 090602.

Saira, O.-P., A. Kemppinen, V. F. Maisi, and J. P. Pekola, 2012, "Vanishing quasiparticle density in a hybrid Al/Cu/Al single-electron transistor," Phys. Rev. B **85**, 012504.

Saira, O.-P., Y. Yoon, T. Tanttu, M. Möttönen, D. V. Averin, and J. P. Pekola, 2012, "Test of the Jarzynski and Crooks Fluctuation Relations in an Electronic System," Phys. Rev. Lett. **109**, 180601.

Saira, Olli-Pentti, Matthias Meschke, Francesco Giazotto, Alexander M. Savin, Mikko Möttönen, and Jukka P. Pekola, 2007, "Heat Transistor: Demonstration of Gate-Controlled Electronic Refrigeration," Phys. Rev. Lett. **99**, 027203.

Sánchez, Rafael, and Markus Büttiker, 2012, "Detection of single-electron heat transfer statistics," Europhys. Lett. **100**, 47008.

Sánchez, Rafael, Björn Sothmann, and Andrew N. Jordan, 2015, "Heat diode and engine based on quantum Hall edge states," New J. Phys. **17**, 075006.

Santamore, D. H., and M. C. Cross, 2001, "Effect of surface roughness on the universal thermal conductance," Phys. Rev. B **63**, 184306.

Scharf, Benedikt, Alessandro Braggio, Elia Strambini, Francesco Giazotto, and Ewelina M. Hankiewicz, 2020, "Topological Josephson heat engine," Commun. Phys. **3**, 198.

Scheibner, R., M. König, D. Reuter, A. D. Wieck, C. Gould, H. Buhmann, and L. W. Molenkamp, 2008, "Quantum dot as thermal rectifier," New J. Phys. **10**, 083016.

Schmidt, D. R., R. J. Schoelkopf, and A. N. Cleland, 2004, "Photon-Mediated Thermal Relaxation of Electrons in Nanostructures," Phys. Rev. Lett. **93**, 045901.

Schwab, K., E. A. Henriksen, J. M. Worlock, and M. L. Roukes, 2000, "Measurement of the quantum of thermal conductance," Nature (London) **404**, 974–977.

Segal, Dvira, and Abraham Nitzan, 2005, "Spin-Boson Thermal Rectifier," Phys. Rev. Lett. **94**, 034301.

Seifert, Udo, 2005, "Entropy Production along a Stochastic Trajectory and an Integral Fluctuation Theorem," Phys. Rev. Lett. **95**, 040602.

Seifert, Udo, 2012, "Stochastic thermodynamics, fluctuation theorems and molecular machines," Rep. Prog. Phys. **75**, 126001.

Senior, Jorden, Azat Gubaydullin, Bayan Karimi, Joonas T. Peltonen, Joachim Ankerhold, and Jukka P. Pekola, 2020, "Heat rectification via a superconducting artificial atom," Commun. Phys. **3**, 40.

Sergi, Danilo, 2011, "Energy transport and fluctuations in small conductors," Phys. Rev. B **83**, 033401.

Silveri, Matti, Hermann Grabert, Shumpei Masuda, Kuan Yen Tan, and Mikko Möttönen, 2017, "Theory of quantum-circuit refrigeration by photon-assisted electron tunneling," Phys. Rev. B **96**, 094524.

Sivan, U., and Y. Imry, 1986, "Multichannel Landauer formula for thermoelectric transport with application to thermopower near the mobility edge," Phys. Rev. B **33**, 551–558.

Sivre, E., A. Anthore, F. D. Parmentier, A. Cavanna, U. Gennser, A. Ouerghi, Y. Jin, and F. Pierre, 2018, "Heat Coulomb blockade of one ballistic channel," Nat. Phys. **14**, 145.

Solfanelli, Andrea, Marco Falsetti, and Michele Campisi, 2020, "Nonadiabatic single-qubit quantum Otto engine," Phys. Rev. B **101**, 054513.

Sothmann, Björn, Rafael Sánchez, Andrew N. Jordan, and Markus Büttiker, 2012, "Rectification of thermal fluctuations in a chaotic cavity heat engine," Phys. Rev. B **85**, 205301.

Srivastav, Saurabh Kumar, Manas Ranjan Sahu, K. Watanabe, T. Taniguchi, Sumilan Banerjee, and Anindya Das, 2019, "Universal quantized thermal conductance in graphene," Sci. Adv. **5**, eaaw5798.

Tan, Kuan Yen, Matti Partanen, Russell E. Lake, Joonas Govenius, Shumpei Masuda, and Mikko Möttönen, 2017, "Quantum-circuit refrigerator," Nat. Commun. **8**, 15189.

Tavakoli, Adib, Christophe Blanc, Hossein Ftouni, Kunal J. Lulla, Andrew D. Fefferman, Eddy Collin, and Olivier Bourgeois, 2017, "Universality of thermal transport in amorphous nanowires at low temperatures," Phys. Rev. B **95**, 165411.

Tavakoli, Adib, Kunal Lulla, Thierry Crozes, Natalio Mingo, Eddy Collin, and Olivier Bourgeois, 2018, "Heat conduction measurements in ballistic 1D phonon waveguides indicate breakdown of the thermal conductance quantization," Nat. Commun. **9**, 4287.

Thomas, George, Jukka P. Pekola, and Dmitry S. Golubev, 2019, "Photonic heat transport across a Josephson junction," Phys. Rev. B **100**, 094508.

Tighe, T. S., J. M. Worlock, and M. L. Roukes, 1997, "Direct thermal conductance measurements on suspended monocrystalline nanostructures," Appl. Phys. Lett. **70**, 2687.

Timofeev, Andrey V., Meri Helle, Matthias Meschke, Mikko Möttönen, and Jukka P. Pekola, 2009, "Electronic Refrigeration at the Quantum Limit," Phys. Rev. Lett. **102**, 200801.

Tinkham, Michael, 2004, *Introduction to Superconductivity*, 2nd ed. (Dover Publications, New York).

van den Berg, Tineke L., Fredrik Brange, and Peter Samuelsson, 2015, "Energy and temperature fluctuations in the single electron box," New J. Phys. **17**, 075012.

van Wees, B. J., H. van Houten, C. W. J. Beenakker, J. G. Williamson, L. P. Kouwenhoven, D. van der Marel, and C. T. Foxon, 1988, "Quantized Conductance of Point Contacts in a Two-Dimensional Electron Gas," Phys. Rev. Lett. **60**, 848–850.

Wang, Haidong, Shiqian Hu, Koji Takahashi, Xing Zhang, Hiroshi Takamatsu, and Jie Chen, 2017, "Experimental study of thermal rectification in suspended monolayer graphene," Nat. Commun. **8**, 15843.

Wang, L. B., O.-P. Saira, D. S. Golubev, and J. P. Pekola, 2019, "Crossover between Electron-Phonon and Boundary-Resistance Limits to Thermal Relaxation in Copper Films," Phys. Rev. Applied **12**, 024051.

Wellstood, F. C., C. Urbina, and John Clarke, 1994, "Hot-electron effects in metals," Phys. Rev. B **49**, 5942–5955.

Wharam, D. A., T. J. Thornton, R. Newbury, M. Pepper, H. Ahmed, J. E. F. Frost, D. G. Hasko, D. C. Peacock, D. A. Ritchie, and G. A. C. Jones, 1988, "One-dimensional transport and the quantisation of the ballistic resistance," J. Phys. C **21**, L209–L214.

Wu, Yong-Shi, 1994, "Statistical Distribution for Generalized Ideal Gas of Fractional-Statistics Particles," Phys. Rev. Lett. **73**, 922–925.

Yung, C. S., D. R. Schmidt, and A. N. Cleland, 2002, "Thermal conductance and electron-phonon coupling in mechanically suspended nanostructures," Appl. Phys. Lett. **81**, 31.

Zen, Nobuyuki, Tuomas A. Puurtinen, Tero J. Isotalo, Saumyadip Chaudhuri, and Ilari J. Maasilta, 2014, "Engineering thermal conductance using a two-dimensional phononic crystal," Nat. Commun. **5**, 3435.

Zhan, Fei, Sergey Denisov, and Peter Hänggi, 2013, "Power spectrum of electronic heat current fluctuations," Phys. Status Solidi B **250**, 2355.

Zhao, Erhai, Tomas Löfwander, and J. A. Sauls, 2003, "Phase Modulated Thermal Conductance of Josephson Weak Links," Phys. Rev. Lett. **91**, 077003.